ARTICLE

Combining endocannabinoids with retigabine for enhanced M-channel effect and improved K_V7 subtype selectivity

Johan E. Larsson[1], Urban Karlsson[1], Xiongyu Wu[2], and Sara I. Liin[1]

Retigabine is unique among anticonvulsant drugs by targeting the neuronal M-channel, which is composed of $K_V7.2$/$K_V7.3$ and contributes to the negative neuronal resting membrane potential. Unfortunately, retigabine causes adverse effects, which limits its clinical use. Adverse effects may be reduced by developing M-channel activators with improved K_V7 subtype selectivity. The aim of this study was to evaluate the prospect of endocannabinoids as M-channel activators, either in isolation or combined with retigabine. Human K_V7 channels were expressed in *Xenopus laevis* oocytes. The effect of extracellular application of compounds with different properties was studied using two-electrode voltage clamp electrophysiology. Site-directed mutagenesis was used to construct channels with mutated residues to aid in the mechanistic understanding of these effects. We find that arachidonoyl-L-serine (ARA-S), a weak endocannabinoid, potently activates the human M-channel expressed in *Xenopus* oocytes. Importantly, we show that ARA-S activates the M-channel via a different mechanism and displays a different K_V7 subtype selectivity compared with retigabine. We demonstrate that coapplication of ARA-S and retigabine at low concentrations retains the effect on the M-channel while limiting effects on other K_V7 subtypes. Our findings suggest that improved K_V7 subtype selectivity of M-channel activators can be achieved through strategically combining compounds with different subtype selectivity.

Introduction

Epilepsy is a disorder of the nervous system that affects an estimated 50 million people worldwide. Although the majority of patients with epilepsy are adequately helped by available treatment (Brodie et al., 2012), over 30% continue to have seizures (Brodie et al., 2012), which motivates major efforts to develop new anti-epileptic treatment strategies. Retigabine was approved by the US Food and Drug Administration in 2011 as the first anti-epileptic drug targeting the neuronal M-channel (Main et al., 2000; Gunthorpe et al., 2012), a potassium channel important for dampening neuronal excitability by contributing to the negative resting membrane potential. Retigabine showed anti-excitable and anti-epileptic effects in cellular and animal models as well as in clinical trials (Rostock et al., 1996; Rundfeldt, 1997; Brodie et al., 2010; French et al., 2011). Retigabine was used as an adjunctive treatment in patients with partial-onset seizures and had advantages, such as less drug interaction with other anticonvulsants, because it is not metabolized through the P-450 system (Hempel et al., 1999; Łuszczki, 2009). Unfortunately, retigabine was associated with adverse effects including

bladder dysfunction and changes in retinal pigmentation (Splinter, 2012; Garin Shkolnik et al., 2014), which limited its clinical use. Retigabine was withdrawn from the market in 2017. Extensive studies using retigabine have established the M-channel as a target for new anti-epileptic drugs but have also highlighted the need to develop strategies to reduce adverse effects of anticonvulsants.

Metabolic instability of retigabine (Groseclose and Castellino, 2019), retigabine effects on M-channels in peripheral nervous tissue (Tykocki et al., 2019), and retigabine off-target effects on other K_V7 channel subtypes (Rode et al., 2010) all likely contribute to adverse effects produced by the drug. The human K_V7 (hK_V7; also called KCNQ) channel family contains a total of five voltage-sensitive potassium channels, h$K_V7.1$ to h$K_V7.5$, which are expressed in various tissues in the body (Robbins, 2001). The M-channel is primarily composed of h$K_V7.2$ and h$K_V7.3$ subunits (Wang et al., 1998), which coassemble as heterotetramers. In some neuronal compartments, h$K_V7.5$ contributes to the M-current (Shah et al., 2002). Retigabine's anti-excitable effect

[1]Department of Biomedical and Clinical Sciences, Linköping University, Linköping, Sweden; [2]Department of Physics, Chemistry and Biology, Linköping University, Linköping, Sweden.

Correspondence to Sara I. Liin: sara.liin@liu.se.

is caused by retigabine binding to a tryptophan in the ion-conducting pore domain of the M-channel (W236 in hK$_V$7.2 and W265 in hK$_V$7.3; Schenzer et al., 2005; Wuttke et al., 2005; Kim et al., 2015), stabilizing the open conformation of the channel. Although hK$_V$7.1 lacks this tryptophan (rendering it insensitive to retigabine), the tryptophan is conserved in hK$_V$7.2–5, which are all activated by retigabine (Schenzer et al., 2005). This poses a potential risk of off-target effects on smooth muscle cells, outer hair cells, and retinal pigment epithelial cells, which have been shown to express hK$_V$7.4 and/or hK$_V$7.5 channels (Holt et al., 2007; Xu et al., 2007; Zhang et al., 2011; Brueggemann et al., 2014; Chadha et al., 2014; Provence et al., 2018).

A means to reduce the adverse effects of retigabine is to improve the metabolic stability and subtype selectivity of retigabine. However, developing retigabine analogues that better differentiate between hK$_V$7 subtypes is challenging because of conserved residues in the retigabine binding site. Moreover, promising retigabine analogues with improved hK$_V$7 subtype selectivity characterized in heterologous cell systems (Kumar et al., 2016) require extensive additional studies before their possible clinical potential is shown. Because retigabine and other M-channel activators could potentially be tolerated in low doses as anti-epileptic drugs, a parallel strategy would be to develop combined treatments to preserve the anticonvulsive M-channel effect while limiting adverse effects. In support of this, Manville and Abbott (2018) elegantly demonstrated that significant activating effects on the M-channel are achieved by a low concentration of retigabine if coapplied with components of herbal extracts binding to a site overlapping with the retigabine site. We hypothesize that the concept of combined targeting of the M-channel with dual drugs could be further developed if retigabine is strategically combined with M-channel activators with K$_V$7 subtype selectivity different from that of retigabine. Specifically, we propose that the subtype selectivity of such a combination treatment could be improved if retigabine is used in conjunction with M-channel activators that act on a site distinct from the retigabine site. In line with this notion, improved drug selectivity with potentially fewer adverse effects is one of the highlighted advantages of positive allosteric modulators targeting ligand-gated ion channels and G protein–coupled receptors (Abdel-Magid, 2015; Changeux and Christopoulos, 2016; Foster and Conn, 2017). These positive allosteric modulators are developed to bind to a site that is distinct from and less conserved than that of the natural ligand, with the aim of enhancing the response of a specific receptor to its ligand.

In this work, we test the potential of endocannabinoids as a novel class of M-channel activators that could be used in conjunction with retigabine. Common endocannabinoids, such as 2-arachidonoylglycerol (2-AG) and N-arachidonoylethanolamine (anandamide; AEA), are composed of an arachidonic acid tail connected to a head group and signal via cannabinoid receptors (Devane et al., 1992; Mechoulam et al., 1995). In addition, several endogenous arachidonic acid–based compounds related to 2-AG and AEA have been identified (Bisogno et al., 2000; Huang et al., 2001; Milman et al., 2006), with weak to strong potential to activate cannabinoid receptors. In this study, we refer to all

these endogenous ligands as "endocannabinoids." Besides the neurobehavioral effects of endocannabinoids mediated through the cannabinoid receptors, there is increasing evidence that endocannabinoids have a broader regulating function in the nervous system through interaction with so-called noncanonical targets. For instance, 2-AG has been shown to increase the firing of dopaminergic neurons by inhibiting A-type potassium channels (Gantz and Bean, 2017). Also, endothelium-dependent relaxation by AEA has been suggested to be caused by direct activation of BK channels (Bondarenko et al., 2017). If also the M-channel is a noncanonical target of endocannabinoids, the different chemical properties of retigabine and endocannabinoids make it likely that endocannabinoids act on a site different from that of retigabine.

We find that specific members of the endocannabinoid family activate the human M-channel (formed by coexpressed hK$_V$7.2 and hK$_V$7.3) expressed in *Xenopus laevis* oocytes. Especially N-arachidonoyl-L-serine (ARA-S), a weak endogenous activator of cannabinoid receptor type 1 (Milman et al., 2006), induced large activating effects at low concentrations. We uncovered that ARA-S acts through a different mechanism and displays a different pattern of hK$_V$7 subtype selectivity compared with that of retigabine. Finally, we demonstrate how to use this by combining low concentrations of ARA-S and retigabine for pronounced activation of the M-channel while limiting activation of the other hK$_V$7 subtypes. Altogether, our study suggests that effective activation of the M-channel with improved hK$_V$7 subtype selectivity can be achieved by strategically combining M-channel activators with additive effects on the M-channel and nonadditive effects on the other hK$_V$7 subtypes.

Materials and methods

All animal experiments were approved by the Linköping Animal Care and Use Committee (Permit #1941) and conform to national and international guidelines.

Test compounds

All chemicals were purchased from Sigma-Aldrich if not stated otherwise. 2-AG, AEA, ARA-S, N-arachidonoyl dopamine (NADA), N-arachidonoyl-γ-aminobutyric acid (NAGABA), arachidonoyl serinol (ARA-Serinol), and N-oleoyl-L-serine (OLE-S) were bought from Cayman Chemicals. Retigabine dihydrochloride was bought from Alomone Labs. N-docosahexaenoyl-L-serine (DOC-S), N-linoleoyl-L-serine (LIN-S), N-arachidonoyl-D-serine, and N-arachidoyl-L-serine (arachidoyl-S) were synthesized in house. The synthesis methods have been partly described previously (Silverå Ejneby et al., 2018). Most of the reagents for synthesis of new compounds were from Sigma-Aldrich except O-(benzotriazol-1-yl)-N,N,N′,N′-tetramethyluronium tetrafluoroborate, which was from Fluka (Fisher Scientific GTH AB). Preparative liquid chromatography (LC) was run on a Waters system with an XSELECT Phenyl-Hexyl column (250 × 19 mm, 5 µm), under neutral condition using gradient CH$_3$CN/water as eluent (A, water phase: 95: 5 water/CH$_3$CN, 10 mM NH$_4$OAc; B, organic phase: 90: 10 CH$_3$CN/water, 10 mM NH$_4$OAc). NMR spectra were recorded on a Varian Avance 300

MHz with solvent indicated. Chemical shift was reported in ppm on the δ scale and referenced to solvents peak (CDCl$_3$: δ$_H$ = 7.26 ppm, δ$_C$ = 77.16 ppm; methanol-d4: δ$_H$ = 3.30 ppm, δ$_C$ = 49.50 ppm).

To the saturated or unsaturated aliphatic acid and 2.20 equiv triethylamine in acetonitrile (20 ml) and/or dimethylformamide (DMF; 2–4 ml) was added 1.05 equiv O-(benzotriazol-1-yl)-N,N,N',N'-tetramethyluronium tetrafluoroborate, and the reaction mixture was stirred at room temperature (rt) for ∼1 h. D-serine or L-serine (1.20 equiv) was added at rt and stirred over 1–7 nights. The solution was concentrated, and 5 ml water was added. The mixture was extracted with ethyl acetate (EA; 5 ml × 3). The organic layers were combined, concentrated, and purified using preparative LC (40–100%). The desired fractions were combined and concentrated to remove most of the acetonitrile. Another 5 ml water was added to the residue. The resulting solution was adjusted to pH at ∼5 using 1 N HCl aqueous solution and extracted with EA (15 ml × 2). The organic layers were concentrated to give the desired product.

DOC-S
Following the general procedure with docosahexaenoic acid (100 mg, 0.304 mmol), L-serine as starting materials, and DMF (2 ml) as solvent, the reaction mixture was stirred overnight at rt, filtered, and purified using preparative LC without extraction to give the product as a syrup (16.8 mg, 13% yield). ^{1}HNMR (CDCl$_3$/CD$_3$OD 3:2, 300 MHz): δ 5.43–5.14 (m, 12H), 4.48 (t, J = 4.2 Hz, 1H), 3.89 (dd, J = 11.4, 4.2 Hz, 1H), 3.76 (dd, J = 11.4, 4.2 Hz, 1H), 2.85–2.57 (m, 12H), 2.39–2.30 (m, 2H), 2.28–2.20 (m, 2H), 2.06–1.92 (m, 2H), 0.90 (t, J = 7.5 Hz, 3H). ^{13}CNMR (CDCl$_3$/CD$_3$OD 3:2, 75 MHz): δ 173.4, 172.2, 131.9, 129.2, 128.4, 128.2, 128.15, 128.1, 128.0, 127.96, 127.9, 127.8, 126.9, 62.4, 54.4, 35.9, 25.5, 25.43, 25.41, 23.1, 20.4, 14.1. MS (ESI$^-$): m/z calcd for C$_{25}$H$_{36}$NO$_4$ (M-H$^-$) 414.26, found 414.51.

LIN-S
Following the general procedure with linoleic acid (280 mg, 0.998 mmol), L-serine (126.1 mg, 1.200 mmol) as starting materials, and acetonitrile (20 ml) as solvent, the reaction mixture was stirred over seven nights at rt, purified using preparative LC to give the product as a syrup (11.1 mg, 3%). ^{1}HNMR (CDCl$_3$, 300 MHz): δ 6.65 (br d, J = 6.6 Hz, 1H, NH), 5.45–5.25 (m, 4H), 4.50 (m, 1H), 4.14 (dd, J = 11.4, 3.6 Hz, 1H), 3.85 (dd, J = 11.4, 3.6 Hz, 1H), 2.82–2.70 (m, 2H), 2.30 (d, J = 7.5 Hz, 2H), 2.15–2.00 (m, 4H), 1.70–1.60 (m, 2H), 1.41–1.20 (m, 14H), 0.87 (t, J = 6.9 Hz, 3H). ^{13}CNMR (CD$_3$OD/CDCl$_3$ 2:1, 75 MHz): δ 175.8, 173.1, 130.7, 130.6, 128.75, 128.69, 62.8, 55.5, 36.8, 32.3, 30.4, 30.11, 30.05, 30.0, 29.9, 27.9, 26.5, 26.3, 23.3, 14.3. MS (ESI$^-$): m/z calcd for C$_{21}$H$_{36}$NO$_4$ (M-H$^-$) 366.26, found 366.41.

Arachidoyl-S
Following the general procedure with arachidic acid (312.5 mg, 1.000 mmol), L-serine (126.1 mg, 1.200 mmol) as starting materials, acetonitrile (20 ml) and DMF (4 ml) as solvents, the reaction mixture was stirred over seven nights at rt. The solubility of this compound is poor. Part of the reaction mixture was purified using preparative LC to give the product as a white solid (5.0 mg). The yield was not calculated. ^{1}HNMR (CDCl$_3$, 300 MHz): δ 4.41 (dd, J = 4.8, 4.2 Hz, 1H), 3.89–3.75 (m, 2H), 2.29–2.22 (m, 2H), 1.35–1.25 (m, 34H), 0.89 (t, J = 7.2 Hz, 3H). MS (ESI$^-$): m/z calcd for C$_{23}$H$_{44}$NO$_4$ (M-H$^-$) 398.33, found 398.67.

N-arachidonoyl-D-serine
Following the general procedure with docosahexaenoic acid (50 mg, 0.164 mmol), D-serine (20.7 mg, 0.197 mmol) as starting materials, and DMF (4 ml) as solvent, the reaction mixture was stirred overnight at rt, filtered, and purified using preparative LC without extraction to give the product as a syrup (21.5 mg, 33% yield). ^{1}HNMR (CDCl$_3$:CD$_3$OD 85:15, 300 MHz): δ 5.40–5.20 (m, 8H), 4.49 (t, J = 3.6 Hz, 1H), 3.89 (dd, J = 11.1, 3.6 Hz, 1H), 3.77 (dd, J = 11.1, 3.6 Hz, 1H), 2.82–2.68 (m, 6H), 2.21 (t, J = 7.8 Hz, 2H), 2.10–1.90 (m, 4H), 1.72–1.58 (m, 2H), 1.36–1.16 (m, 6H), 0.82 (t, J = 6.6 Hz, 3H). ^{13}CNMR (CDCl$_3$:CD$_3$OD 85:15, 75 MHz): δ 174.1, 172.4, 130.5, 129.0, 128.8, 128.6, 128.3, 128.2, 127.9, 127.5, 62.6, 54.5, 35.7, 31.5, 29.3, 27.2, 26.7, 25.6, 25.0, 22.5, 14.0. MS (ESI$^-$): m/z calcd for C$_{23}$H$_{36}$NO$_4$ (M-H$^-$) 390.26, found 390.60.

All compounds were either delivered as or diluted as ethanol stock solutions except for 2-AG, which was delivered in acetonitrile. Stock solutions were stored at –20°C except for 2-AG, which was stored at –80°C.

Two-electrode voltage clamp electrophysiology on
***Xenopus* oocytes**
Xenopus oocytes were surgically isolated and prepared at Linköping University alternatively purchased from Ecocyte Bioscience. Isolated *Xenopus* oocytes were injected with 50 nl RNA. Each oocyte was injected with 2.5 ng of hK$_V$7.2 (GenBank accession no. NM_004518) and 2.5 ng of hK$_V$7.3 (GenBank accession no. NM_004519) RNA for hK$_V$7.2/3. For other channels, 2.5–50 ng of RNA was injected per oocyte (GenBank accession nos. NM_000218 for hK$_V$7.1; NM_004700 for hK$_V$7.4; and NM_001160133 for hK$_V$7.5). Sequence alterations were introduced using site-directed mutagenesis (QuikChange II XL with 10 XL Gold cells; Agilent), and constructs were sequenced at the Core Facility at Linköping University to ensure correct sequence. cRNA was prepared using a T7 mMessage mMachine transcription kit (Invitrogen). RNA concentration was quantified using spectrophotometry (NanoDrop 2000c, Thermo Scientific). Injected oocytes were incubated at 8°C or 16°C for 2–4 d before being used for experiments. The two-electrode voltage clamp recordings were performed using a Dagan CA-1B Amplifier (Dagan). Currents were filtered at 500 Hz and sampled at 5 kHz. The holding voltage was generally set to –80 mV. Activation curves were generally generated in steps between –100 and +50 mV in increments of 10 mV (2-s duration). The tail voltage was generally set to –30 mV. In experiments where a large shift in half-maximal activation (V_{50}) occurred, a prepulse to –140 mV, –120 mV, or –100 mV (2-s duration) was included before the test voltage steps to close the channels. The control solution contained 88 mM NaCl, 1 mM KCl, 15 mM HEPES, 0.4 mM CaCl$_2$, and 0.8 mM MgCl$_2$. pH was set to 7.4 using NaOH. When experiments were performed at lower or higher pH, pH was set the same day as the experiment using HCl or NaOH, respectively. The two-electrode voltage clamp recordings were performed at rt. Control and test solutions (with endocannabinoids or/and

retigabine or ICA73) were applied continuously using a pump (model ISM597D; Labinett Lab AB) with a perfusion rate of 0.5 ml/min during all recordings. Test solution was applied during an application protocol (depolarizing steps to –40 mV every 10 s) to ensure steady-state effects. If no effect was observed during application, the compound was applied for a minimum of 5 min.

Electrophysiological analysis

GraphPad Prism 6 and 7 were used for the electrophysiological analysis. Tail currents were measured shortly after stepping to the tail voltage and plotted against the preceding test voltage to approximate voltage dependence of the channels. A Boltzmann function was fitted to the data to generate the conductance versus voltage ($G(V)$) curve:

$$G(V) = Bottom + (Top - Bottom) \Big/ \left\{ 1 + \exp\left[\frac{(V_{50} - V)}{s}\right] \right\}, \quad (1)$$

where $Bottom$ is the minimal conductance, Top is the maximal conductance, V_{50} is the midpoint (i.e., the voltage needed to reach half the maximal conductance determined from the fit), and s is the slope of the curve. s was constrained to be equal for control and test curves in each oocyte. The difference in V_{50} induced by the test compound in each oocyte (i.e., ΔV_{50}) was used to quantify the shift in the voltage dependence for channel opening. In some figures, $G(V)$ curves have been normalized to the G_{MAX} of control for clarity of the shift of voltage dependence. Basic biophysical properties of studied channels are provided in Table S1.

To plot the concentration dependence or pH dependence of the effect (ΔE) on V_{50} or G_{MAX} as a function of the compound or H^+ concentration (c), the following concentration-response curve was fitted to the data:

$$\Delta E = E_{MAX} \Big/ \left[1 + \left(\frac{EC_{50}}{C}\right)^N \right], \quad (2)$$

where E_{MAX} is the maximal effect on V_{50} or G_{MAX}, EC_{50} the concentration needed to cause 50% of the maximal effect, and N the Hill coefficient. ARA-S effects on opening and closing kinetics were determined by fitting a single exponential function to the first 500 ms of the current triggered by a depolarizing or hyperpolarizing pulse (as specified in the text) and determining the ratio of the time constant, τ, in the presence and absence of ARA-S. These experiments were performed in high K^+ solution (100 mM K^+).

Statistical analysis

Average values are expressed as mean ± SEM. Statistical analyses were done using one-way ANOVA followed by a multiple comparison test when comparing multiple data points. Dunnett's multiple comparisons test was used when compared to defined reference data. Statistical analyses were done using Student's t test when comparing two data points against each other or against a hypothetical value of zero. $P < 0.05$ was considered statistically significant. In case of a large number of Student's t tests, the significance level was adjusted with a Bonferroni correction to reduce the risk of a type 1 error.

Online supplementary material

Fig. S1 shows that specific endocannabinoids do not activate the $hK_V7.2/3$ channel. Fig. S2 shows the effect of ARA-S and NAGABA on $hK_V7.2/3$. Fig. S3 shows the effect of N-arachidonoyl-D-serine on $hK_V7.2/3$. Fig. S4 shows that ARA-S activates homomeric $hK_V7.2$ and $hK_V7.3$ tryptophan mutants. Fig. S5 shows that the specific charge-neutralizing mutation in $hK_V7.2$ reduces ARA-S effect. Fig. S6 shows that the specific charge-neutralizing mutation in $hK_V7.3$ reduces ARA-S effect. Fig. S7 shows that coapplication of low concentrations of ARA-S and retigabine limits the off-target effect on other hK_V7 subtypes. Fig. S8 shows that coapplication of low concentrations of ARA-S and ICA73 limits the off-target effect on other hK_V7 subtypes. Table S1 summarizes the biophysical properties of used constructs.

Results

ARA-S and NAGABA activate $hK_V7.2/3$

To study whether endocannabinoids target the M-channel, we initially tested the effect of five arachidonic acid–based endocannabinoids on $hK_V7.2$ and $hK_V7.3$ coexpressed in *Xenopus* oocytes (hereafter referred to as $hK_V7.2/3$): 2-AG, AEA, ARA-S, NADA, and NAGABA (Fig. 1 a). All five compounds share an arachidonic acid tail (which makes them likely to be among the more prevalent endocannabinoids because of the high abundance of arachidonic acid in membranes; Di Marzo et al., 2004) yet contain diverse head groups (which may indicate different functional effects; Bohannon et al., 2020). Each compound was applied at two concentrations, 10 µM and 100 µM. From this initial screen, we identified two compounds that activated the $hK_V7.2/3$ channel. 10 µM and 100 µM ARA-S and NAGABA significantly shifted the voltage for V_{50} toward negative voltages (Fig. 1 b), thus allowing the channel to open at more negative voltages. ARA-S also significantly increased the maximal conductance (G_{MAX}; Fig. 1 c). In contrast, 2-AG, AEA, and NADA had no effect on V_{50} or G_{MAX} of the $hK_V7.2/3$ channel (Fig. 1, b and c; and Fig. S1, a–c).

ARA-S potently modulates the $hK_V7.2/3$ channel

We investigated the activating effects of ARA-S and NAGABA further. 10 µM ARA-S induced a clear increase in the overall current amplitude of $hK_V7.2/3$ (Fig. 1 d). The onset of the ARA-S effect was relatively fast, with stable effects achieved within 2 min (Fig. S2 a). The washout of the ARA-S effect using control solution was relatively slow, with roughly 10 min of washout required for full reversibility (Fig. S2 b). The washout was faster when albumin, which binds endocannabinoids (Bojesen and Hansen, 2003), was added to the control solution (Fig. S2 b). ARA-S sped up channel-opening kinetics and slowed down the closing kinetics (Fig. S2 c; for opening at +20 mV, τ_{ARA-S}/τ_{ctrl} = 0.76 ± 0.02; for closing at –100 mV, τ_{ARA-S}/τ_{ctrl} = 1.45 ± 0.11; n = 3). The conductance versus voltage ($G(V)$) curve clearly demonstrates the ability of ARA-S to shift V_{50} and increase G_{MAX}
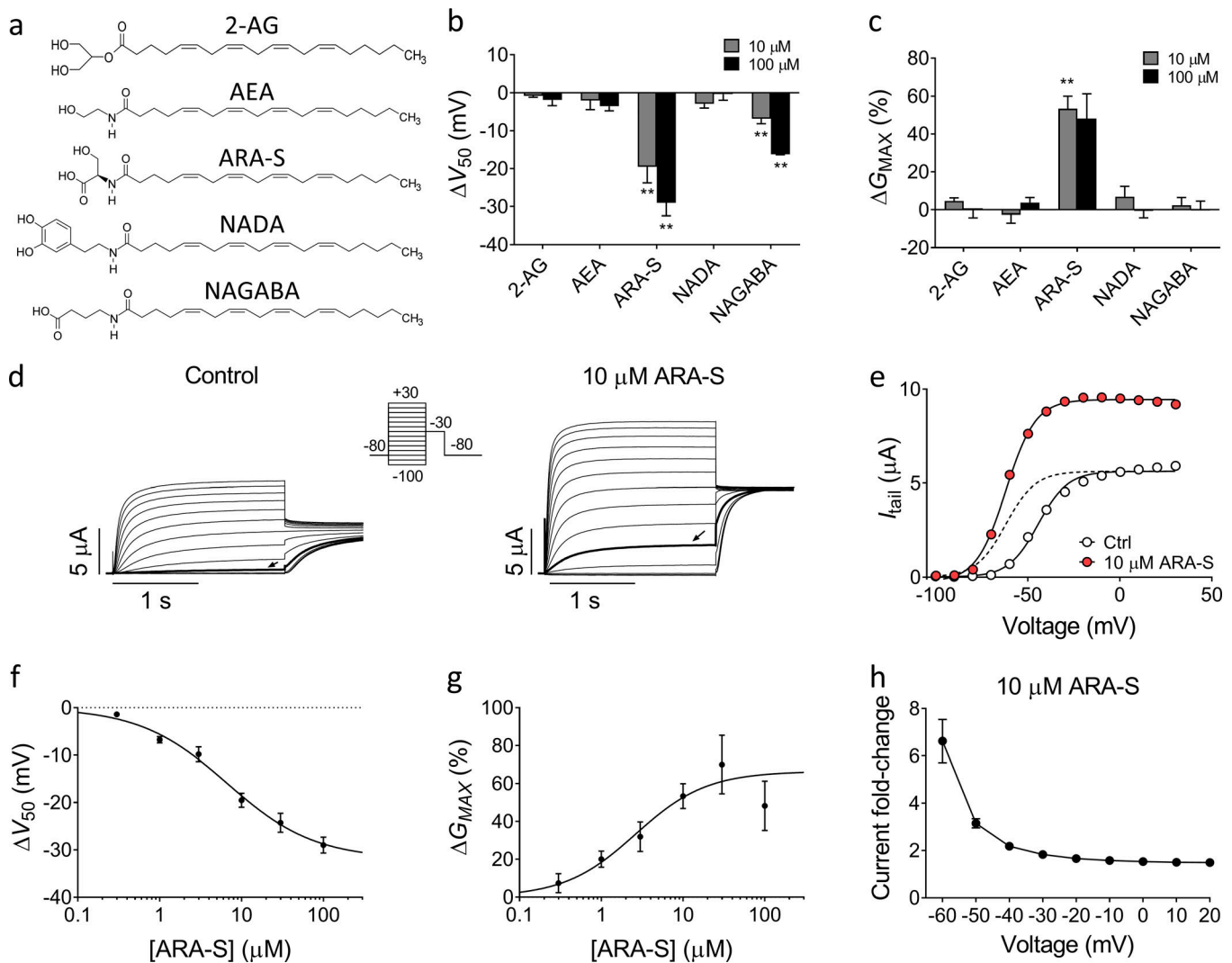
Larsson et al.
Combined targeting of the M-channel

Journal of General Physiology   4 of 15
https://doi.org/10.1085/jgp.202012576

Figure 1. **Specific endocannabinoids activate the hK$_V$7.2/3 channel expressed in *Xenopus* oocytes. (a)** Molecular structure of 2-AG, AEA, ARA-S, NADA, and NAGABA. **(b and c)** Mean shift in V_{50} (ΔV_{50}; b) and mean increase in G_{MAX} (ΔG_{MAX}; c) induced by 10 or 100 µM of indicated endocannabinoid on hK$_V$7.2/3. Data shown as mean ± SEM; n = 4–8. Statistics denote Student's *t* test compared with a hypothetical value of 0 with a Bonferroni corrected significance value of P < 0.005. ** indicates P < 0.001. **(d)** Representative current traces of hK$_V$7.2/3 before and after application of 10 µM ARA-S. Arrow indicates an activating voltage step to −60 mV. Insert of used voltage clamp protocol. **(e)** Representative $G(V)$ curve for the effect of 10 µM ARA-S for the cell shown in d. Dashed line shows the curve for 10 µM ARA-S normalized to G_{MAX} of control. **(f)** Concentration-response relation for ARA-S effect on V_{50}. Data shown as mean ± SEM; n = 4–11. $\Delta V_{50:MAX}$ (maximal shift in V50) = −32 mV; EC$_{50}$ = 7 µM. **(g)** Concentration-response relation for ARA-S effect on G_{MAX}. Data shown as mean ± SEM; n = 4–10. $\Delta G_{MAX:MAX}$ (maximal increase of G_{MAX}) = 66%; EC$_{50}$ = 3 µM. **(h)** Mean hK$_V$7.2/3 current fold increase at different voltages induced by 10 µM ARA-S. Data shown as mean ± SEM; n = 8.

(Fig. 1 e). On average, 10 µM ARA-S shifted V_{50} by −19.5 ± 1.5 mV and increased G_{MAX} by 53% ± 7%. The shift in V_{50} induced by ARA-S was significant at concentrations as low as 300 nM (−1.4 ± 0.4 mV, P = 0.03 using Student's *t* test; Fig. 1 f). The concentration-response curve for the V_{50} effect of ARA-S suggests an estimated maximal shift of V_{50} by −31.9 ± 4.3 mV with 50% of the maximal shift (EC$_{50}$) caused by 7 µM (Fig. 1 f). The concentration-response curve for the G_{MAX} effect of ARA-S suggests an estimated maximal increase of G_{MAX} by 66% ± 8%, with an EC$_{50}$ of 3 µM (Fig. 1 g). Both the shift in V_{50} and the increase in G_{MAX} occur at similar concentrations and together contribute to the overall increase of the current. On average, 10 µM ARA-S induced a sevenfold increase in the current at

−60 mV (Fig. 1 h), suggesting that ARA-S effectively activates hK$_V$7.2/3 at voltages around the resting membrane potential of neurons.

NAGABA produced overall similar but smaller effects compared with ARA-S (Fig. S2, d–g). On average, 10 µM NAGABA shifted V_{50} by −6.9 ± 0.5 mV but did not significantly increase G_{MAX}. The concentration-response curve for the V_{50} effect of NAGABA suggests an estimated maximal shift of V_{50} by −20.8 ± 5.2 mV with an EC$_{50}$ of 24 µM (Fig. S2 e). A concentration-response curve for the G_{MAX} effect of NAGABA could not be obtained as there was no consistent effect of NAGABA on G_{MAX} (Fig. S2 f). On average, 10 µM NAGABA induced a threefold increase in the current at −60 mV (Fig. S2 g).

The charge of the endocannabinoid head group is essential for the activating effect

We tested which molecular determinants of the studied endocannabinoids are necessary to induce activating effects on the hK$_V$7.2/3 channel. Modifying either the head or the lipid tail of the endocannabinoid could potentially change the effect of the compound. For instance, the head group of both ARA-S and NAGABA contains a carboxyl group, which can lose a proton to become negatively charged depending on the acid dissociation constant (pKa) of the head group and the pH of the surrounding solution. To test whether the negative charge of the head group is important for the ARA-S effect, we tested ARA-Serinol, which has a head group that lacks the carboxyl group of ARA-S and therefore is uncharged (Fig. 2 a). 10 µM ARA-Serinol had no significant effect on V_{50} or G_{MAX} of hK$_V$7.2/3 (Fig. 2, a–c; P > 0.05 using Student's t test), suggesting that the carboxyl group is required for the activating effect.

We tested the effect of ARA-S and NAGABA on V_{50} at different extracellular pH to alter the degree of carboxyl group protonation. For ARA-S, the effect on V_{50} was not increased when pH levels were increased from pH 7.4 to pH 9.0 or 10 (Fig. 2 d). However, the effect was reduced when pH was decreased from pH 7.4 to pH 5.5 (Fig. 2 d). The estimated apparent pKa for ARA-S at the channel is 5.4 (Fig. 2 d), which suggests that ARA-S is fully deprotonated at physiological pH. In contrast, the effect of NAGABA was increased when pH was increased from pH 7.4 to pH 9.0 or 10, and the effect of NAGABA was eliminated when pH was decreased from pH 7.4 to pH 6.5 (Fig. 2 e). The estimated apparent pKa for NAGABA at the channel is 7.3 (Fig. 2 e), suggesting that only around 50% of the NAGABA molecules are deprotonated at physiological pH. The difference in estimated pKa could partly explain the difference in effect of ARA-S and NAGABA on V_{50} at pH 7.4.

Since the head group of ARA-S contains a serine moiety, ARA-S could be either L or D enantiomer. The naturally occurring enantiomer (Milman et al., 2006) tested in the initial experiments was the L enantiomer of ARA-S. To test if the chirality affects the effect of ARA-S on hK$_V$7.2/3, we tested the D enantiomer of ARA-S. The D enantiomer of ARA-S induced effects comparable to those of the L enantiomer on V_{50} and G_{MAX} of hK$_V$7.2/3 (Fig. S3, a–c). Altogether, these findings suggest that the negative charge of the endocannabinoid head group is important for the activating effect on the hK$_V$7.2/3 channel, but not the chirality of the head. The importance of the negative charge could explain why 2-AG, AEA, and NADA do not activate the hK$_V$7.2/3 channel, as none of these compounds can be negatively charged.

The composition of the fatty acid tail alters the effect

We next tested the impact of the fatty acid tail on the effect of ARA-S on hK$_V$7.2/3. We kept the serine head but exchanged the arachidonic acid tail of ARA-S to different lipid tails. We tested the polyunsaturated docosahexaenoic and linoleic tails (DOC-S and LIN-S), the monounsaturated oleic tail (OLE-S), and the saturated arachidic tail (arachidoyl-S; Fig. 2 f). At a concentration of 10 µM, exchanging the arachidonic tail for the docosahexaenoic tail preserved the ability to shift V_{50} and increase

G_{MAX} (Fig. 2, g and h). The linoleic tail reduced the ability to shift V_{50} but preserved the ability to increase G_{MAX} (Fig. 2, g and h). The oleic tail reduced the ability to shift both V_{50} and increase G_{MAX} (Fig. 2, g and h). The arachidic tail eliminated the activating effect on hK$_V$7.2/3 (Fig. 2, g and h). Altogether, these data suggest that the composition of the lipid tail alters the effect on hK$_V$7.2/3. Decreasing the number of double bonds in the fatty acid tail tended to decrease the effect of the serine compounds on hK$_V$7.2/3. It should be noted that arachidoyl-S was difficult to dissolve, suggesting that the absence of effect of arachidoyl-S could be caused in part by poor solubility.

ARA-S and retigabine activates hK$_V$7.2/3 through different mechanisms

As previously described, retigabine (structure in Fig. 3 a) shifts V_{50} of hK$_V$7.2/3 to negative voltages and increases the overall current (Main et al., 2000). In our experiments, retigabine shifted V_{50} of hK$_V$7.2/3 with an estimated EC$_{50}$ of 2 µM and a ΔV_{50} of −21.7 ± 0.5 mV induced by 3 µM retigabine (Fig. 3, a and b). As has been previously demonstrated (Schenzer et al., 2005), removing the tryptophan in S5 that is important for retigabine effects (by constructing the hK$_V$7.2_W236L and hK$_V$7.3_W265L mutants and coexpressing them as hK$_V$7.2_W236L/hK$_V$7.3_W265L) rendered the channel insensitive to 3 µM retigabine (Fig. 3, c and d). ARA-S, on the other hand, retained its effect on the hK$_V$7.2_W236L/hK$_V$7.3_W265L channel (Fig. 3, e and f) as well as on homomeric hK$_V$7.2_W236L and hK$_V$7.3_W265L channels (Fig. S4, a–d). These experiments demonstrate that the tryptophan in S5 is not important for the activating effect of ARA-S and suggest that ARA-S and retigabine activate the channel through distinct mechanisms. Moreover, ARA-S retained its effect on the hK$_V$7.2_F168L channel (Fig. S4, e and f), which was previously shown to render the channel insensitive to the M-channel activator ICA73 (ICA-069673) by removing the phenylalanine in S3 (Wang et al., 2017; Wang et al., 2018). This suggests that ARA-S activates the channel through a mechanism different from that of ICA73.

Positively charged residues in S4 and S6 are important for ARA-S–induced activation

In previous work, we showed that polyunsaturated fatty acids and their analogues activate K$_V$ channels (Liin et al., 2015; Liin et al., 2016; Elinder and Liin, 2017). In hK$_V$7.1, we have suggested that the activation is caused by two distinct interactions between polyunsaturated fatty acids and the channel (Liin et al., 2018): (1) interaction with the outermost arginines in S4 of the voltage-sensing domain facilitates outward S4 movement to shift V_{50} toward more negative voltages (illustrated in Fig. 4 a, top row), and (2) interaction with a lysine in S6 of the pore domain increases G_{MAX}, possibly by stabilizing the conducting selectivity filter (illustrated in Fig. 4 a, bottom row). Both the negative charge of the fatty acid and the polyunsaturation of the lipid tail are important for these effects (Börjesson et al., 2008; Börjesson and Elinder, 2011; Liin et al., 2015; Bohannon et al., 2019). Because of the similarity in chemical properties of polyunsaturated fatty acids and endocannabinoids and their overall similar pattern of chemical properties required to activate K$_V$7 channels, we tested whether the corresponding residues in
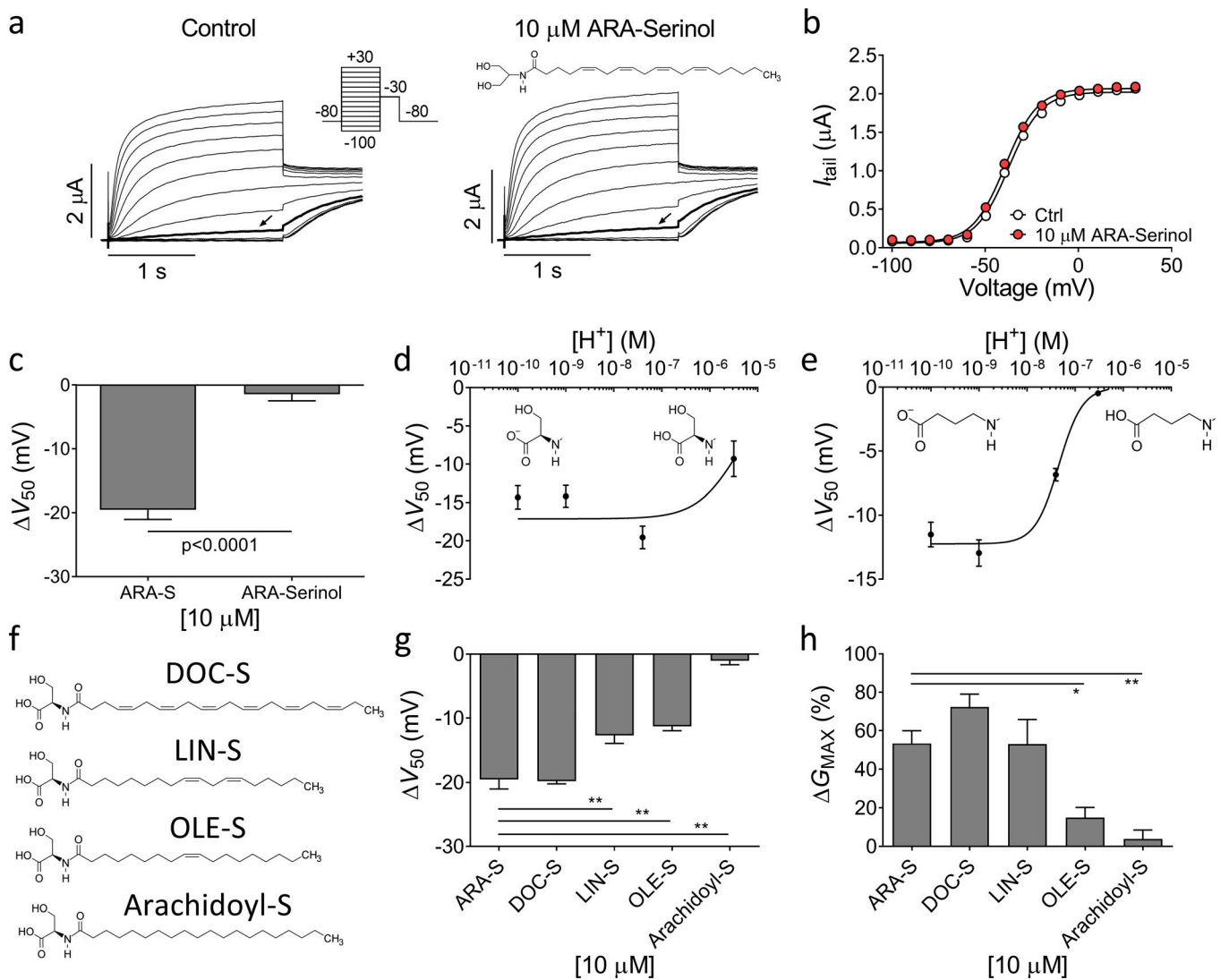
Larsson et al.
Combined targeting of the M-channel

Journal of General Physiology   6 of 15
https://doi.org/10.1085/jgp.202012576

Figure 2. **Importance of the negative charge of the head group and composition of lipid tail for endocannabinoid effect on hK$_V$7.2/3. (a)** Representative current traces of hK$_V$7.2/3 before and after application of 10 µM ARA-Serinol. Arrow indicates an activating voltage step to –50 mV. Insert of used voltage clamp protocol and molecular structure of ARA-Serinol. **(b)** Representative $G(V)$ curve for the effect of 10 µM ARA-Serinol for the cell shown in a. **(c)** Mean ΔV_{50} induced by 10 µM ARA-S or 10 µM ARA-Serinol. Data shown as mean ± SEM; n = 4–8. **(d)** pH response relation for 10 µM ARA-S effect on V_{50}. Data shown as mean ± SEM; n = 3–8. Apparent pKa = 5.4. Inserts indicate the structure of deprotonated and protonated ARA-S head. **(e)** pH response relation for 10 µM NAGABA effect on V_{50}. Data shown as mean ± SEM; n = 4–7. Apparent pKa = 7.3. Inserts indicate the structure of deprotonated and protonated NAGABA head. **(f)** Molecular structure of DOC-S, LIN-S, OLE-S, and arachidoyl-S. **(g and h)** Mean ΔV_{50} (g) and ΔG_{MAX} (h) induced by 10 µM indicated serine endocannabinoid analogues. Data shown as mean ± SEM; n = 5–9. Statistics denote one-way ANOVA with Dunnett's multiple comparison test with ARA-S set as control. * indicates P < 0.01; ** indicates P < 0.001.

hK$_V$7.2 and hK$_V$7.3 are important for the ARA-S effect. In hK$_V$7.2, neutralization of either the first or second S4 arginine (R198 and R201, respectively) significantly reduced the ability of 10 µM ARA-S to shift V_{50} (Fig. 4 b and Fig. S5). Note that the Q204R mutation was introduced together with the R201Q mutation, as the R201Q single mutant is voltage insensitive (Miceli et al., 2008). Guided by studies in hK$_V$7.1 (Panaghie and Abbott, 2007; Wu et al., 2010), we found that voltage sensitivity of the R201Q mutant was retained by introducing a compensatory positive charge at the Q204 position, which allowed probing of ARA-S effects on V_{50} of this mutant. The Q204R mutation per se did not appear to alter

the ARA-S effect on V_{50} (compare effects on R198Q and R198Q/Q204R in Fig. 4 b). In contrast, neutralization of R291 in S6 (corresponding to the lysine in S6 of hK$_V$7.1) significantly reduced the ability of 10 µM ARA-S to increase G_{MAX} (Fig. 4 c and Fig. S5). In hK$_V$7.3, neutralization of either the first or second S4 arginine (R227 and R230, respectively) alone did not alter the ARA-S effect on V_{50} (Fig. 4 d and Fig. S6). However, simultaneous neutralization of R227 and R230 significantly reduced the ability of 10 µM ARA-S to shift V_{50} (Fig. 4 d and Fig. S6). As with hK$_V$7.2, a compensatory positive charge at the Q233 position was introduced to retain voltage sensitivity.
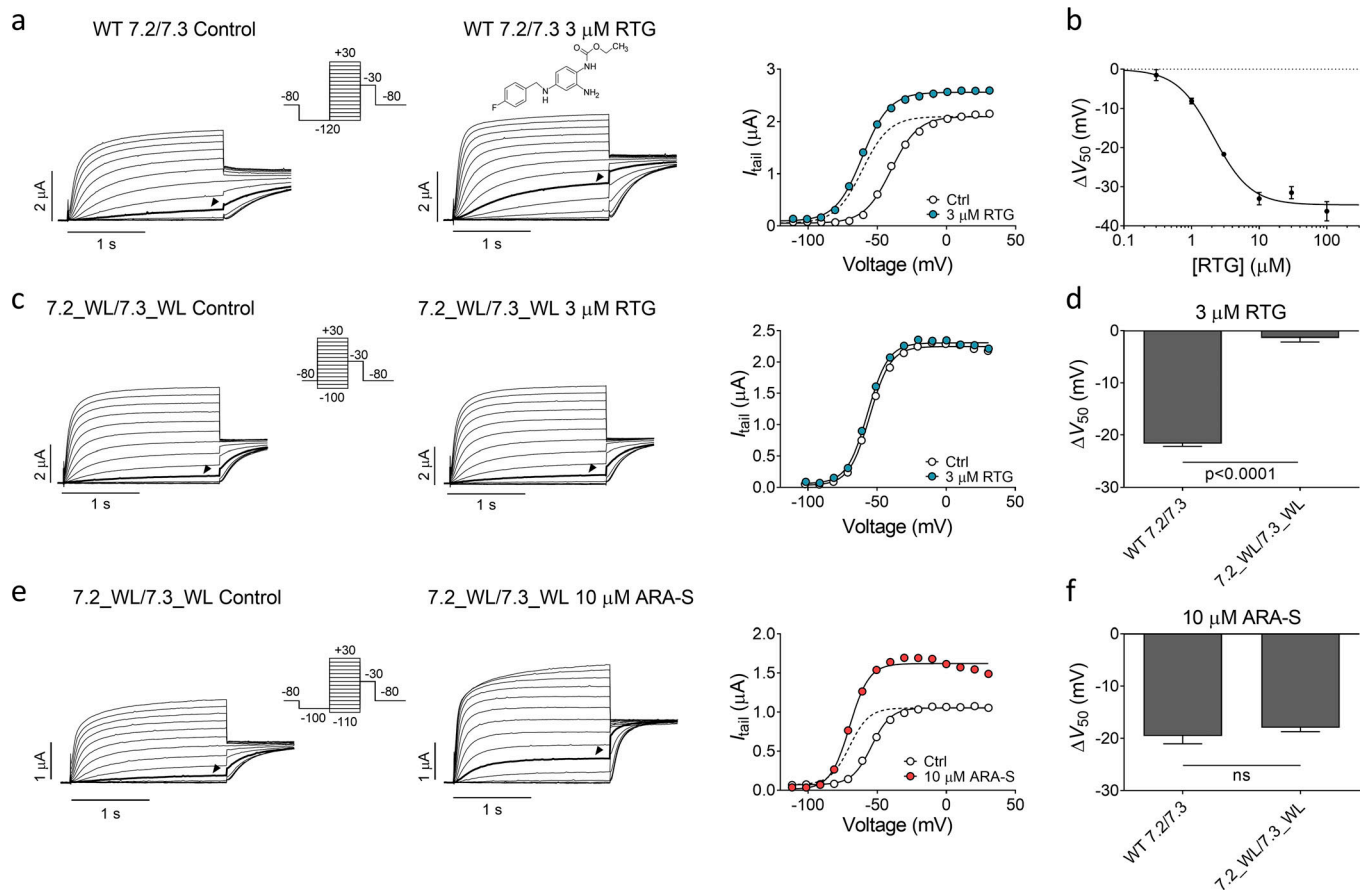
Figure 3.   **ARA-S and retigabine activate hK$_V$7.2/3 through different mechanisms. (a)** Representative current traces and corresponding $G(V)$ curve of hK$_V$7.2/3 before and after application of 3 µM retigabine (RTG). Arrowheads in the current families indicate an activating voltage step to −50 mV. Insert of used voltage clamp protocol. Dashed line shows the curve for 3 µM retigabine normalized to G_{MAX} of control. **(b)** Concentration-response relation for retigabine effect on V_{50}. Data shown as mean ± SEM; n = 4–7. $\Delta V_{50:MAX \text{ (maximal shift in } V_{50})}$ = −35 mV; EC$_{50}$ = 2 µM. **(c)** Same as in a, but for hK$_V$7.2_W236L/hK$_V$7.3_W265L. Arrowheads indicate an activating voltage step to −60 mV. **(d)** Mean shift in V_{50} induced by 3 µM retigabine on WT hK$_V$7.2/3 or hK$_V$7.2_W236L/hK$_V$7.3_W265L. Data shown as mean ± SEM; n = 4 or 5. Statistics denote Student's t test. **(e)** Same as in c, but for the effect of 10 µM ARA-S on hK$_V$7.2_W236L/hK$_V$7.3_W265L. Arrowheads indicate an activating voltage step to −60 mV. **(f)** Mean shift in V_{50} induced by 10 µM ARA-S on WT hK$_V$7.2/3 or hK$_V$7.2_W236L/hK$_V$7.3_W265L. Data shown as mean ± SEM; n = 5–8. Statistics denote Student's t test. ns, nonsignificant; WL, tryptophan to leucine mutation.

For hK$_V$7.3, the effect of mutation on G_{MAX} was less clear, with no significant reduction in the ability of 10 µM ARA-S to increase G_{MAX} by the R330Q mutation (Fig. 4 e and Fig. S6). However, interpretation of alteration in the G_{MAX} effect in hK$_V$7.3 is possibly complicated by the A315T mutation introduced to enable studies of homotetrameric hK$_V$7.3 channels. The A315T mutations have been proposed to increase the K$^+$ current generated by hK$_V$7.3 by stabilizing the conducting pore (Choveau et al., 2012a, 2012b), possibly together with increasing membrane expression (Gómez-Posada et al., 2010). Because the ARA-S effect on G_{MAX} is expected to be dependent on the intrinsic open probability of the channel (Liin et al., 2018), possible varying intrinsic open probability of the hK$_V$7.3 mutants will impact the ability of ARA-S to increase G_{MAX}. Altogether, experiments on the set of mutants with neutralized positive residues at specific positions suggest that positively charged amino acids in S4 and S6 are important for the ability of ARA-S to shift V_{50} (in both hK$_V$7.2 and hK$_V$7.3) and increase G_{MAX} (in hK$_V$7.2), respectively.

ARA-S displays a different K$_V$7 subtype selectivity than retigabine

Retigabine was previously shown to activate all members within the hK$_V$7 family except hK$_V$7.1 (Tatulian et al., 2001; Schenzer et al., 2005). Because our results indicate that the activation of hK$_V$7.2/3 induced by ARA-S and retigabine occurs via different mechanisms, ARA-S might show a different hK$_V$7 subtype selectivity than retigabine. We tested the effect of ARA-S on each member of the hK$_V$7 channel family expressed as homomeric channels in *Xenopus* oocytes. 10 µM ARA-S significantly activated hK$_V$7.1, hK$_V$7.2, hK$_V$7.3_A315T, and hK$_V$7.5 by shifting V_{50} toward more negative voltages and increasing G_{MAX} (Fig. 5, a–c and e–g). In contrast, ARA-S had a slight inhibiting effect on hK$_V$7.4. 10 µM ARA-S shifted V_{50} of hK$_V$7.4 by +6.7 ± 2.0 mV (Fig. 5 dFig. 5, d and f; P < 0.009 with Student's t test) but had no effect on G_{MAX} (Fig. 5 g). Fig. 5, h and i shows the corresponding effects of 3 µM retigabine on V_{50} and G_{MAX}, which are in overall concordance with previously reported effects for this retigabine concentration (Schenzer et al., 2005). Altogether, these experiments reveal that ARA-S has a different subtype selectivity in its
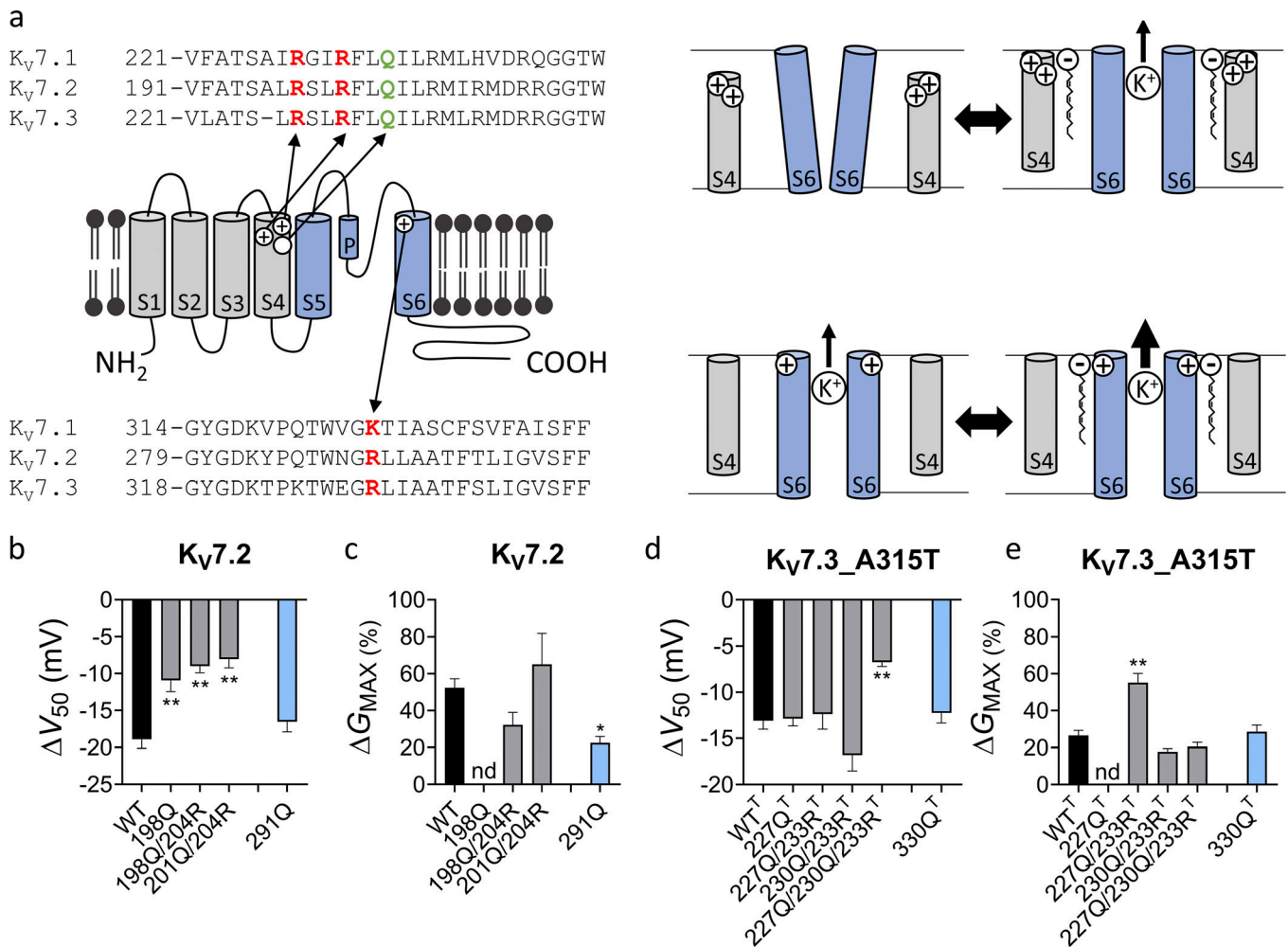
Figure 4. **Positively charged residues in S4 and S6 are important for ARA-S activation of hK$_V$7.2 and hK$_V$7.3. (a)** Schematic side view of one hK$_V$7 subunit. Transmembrane segments S1–S4, forming the voltage sensor domain, are in gray, and transmembrane segments S5 and S6, forming the pore domain, are in blue. P denotes the pore helix. Amino acid sequences for hK$_V$7.1, hK$_V$7.2, and hK$_V$7.3 are shown above (S4) and below (S6) the channel. Residues mutated to study the ARA-S mechanism of action are indicated in the schematic channel model and sequences. These residues were selected based on previous work identifying residues important for polyunsaturated fatty acid effects on hK$_V$7.1 (Liin et al., 2018). A similar mechanism of action was hypothesized for ARA-S. Top right: the negative charge of the ARA-S head interacts with the first and/or second top arginines of S4 (often called "R1" and "R2," indicated in red in the S4 sequence) to facilitate the outward movement of S4. S4 movement triggers channel opening. Lower right: In addition, the negative charge of the ARA-S head interacts with the lysine/arginine in the top of S6 (indicated in red in the S6 sequence) to stabilize the selectivity filter in the pore, which increases the overall K$^+$ conductance. Note that hK$_V$7 channels have a glutamine in the natural spot for the third S4 arginine ("Q3," indicated in green in the S4 sequence). For certain constructs, an arginine was introduced in the Q3 position to restore voltage sensitivity or shift the voltage sensitivity to more WT-like voltages. **(b and c)** Mean ΔV_{50} (b) and ΔG_{MAX} (c) induced by 10 µM ARA-S on hK$_V$7.2 with indicated amino acid substitutions. Data shown as mean ± SEM; n = 6–10. Statistics denote one-way ANOVA with Dunnett's multiple comparison test with WT set as control. The Q204R mutation was introduced to retain voltage sensitivity (see main text for details). nd denotes not determined, as G_{MAX} could not be reliably determined for the R198Q mutant. **(d and e)** Same as in b and c, but for hK$_V$7.3_A315T with indicated amino acid substitutions (^{T} denotes the substitution of A315T in the constructs). n = 4–9. Statistics denote one-way ANOVA with Dunnett's multiple comparison test with WT^T set as control. The Q233R mutation was introduced to retain voltage sensitivity (see main text for details). nd denotes not determined, as G_{MAX} could not be reliably determined for the R227Q mutant. * indicates $P < 0.05$; ** indicates $P < 0.001$.

effect on the hK$_V$7.1 and hK$_V$7.4 channels compared with retigabine.

Significant activating effects on hK$_V$7.2/3 when coapplying low concentrations of ARA-S and retigabine

We hypothesized that one could leverage upon the similar effect of ARA-S and retigabine on the M-channel and the different effect on the other hK$_V$7 subtypes by coapplying low concentrations of ARA-S and retigabine for retained M-channel effect with limited off-target effects. As a first step, we compared the

effect of low concentrations of ARA-S or retigabine alone with both compounds in combination on hK$_V$7.2/3. 1 µM ARA-S alone shifted V_{50} of hK$_V$7.2/3 by −6.7 ± 0.7 mV and increased G_{MAX} by 20% ± 4% (Fig. 6). 1 µM retigabine alone shifted V_{50} of hK$_V$7.2/3 by −8.1 ± 0.7 mV and did not affect G_{MAX} (Fig. 6). In contrast, coapplication of 1 µM ARA-S and 1 µM retigabine shifted V_{50} by −19.5 ± 1.3 mV and increased G_{MAX} by 31% ± 9% (Fig. 6). The improved effect of coapplication of low concentrations of ARA-S and retigabine was clear when comparing the magnitude of hK$_V$7.2/3 current fold increase at negative voltages. On average,
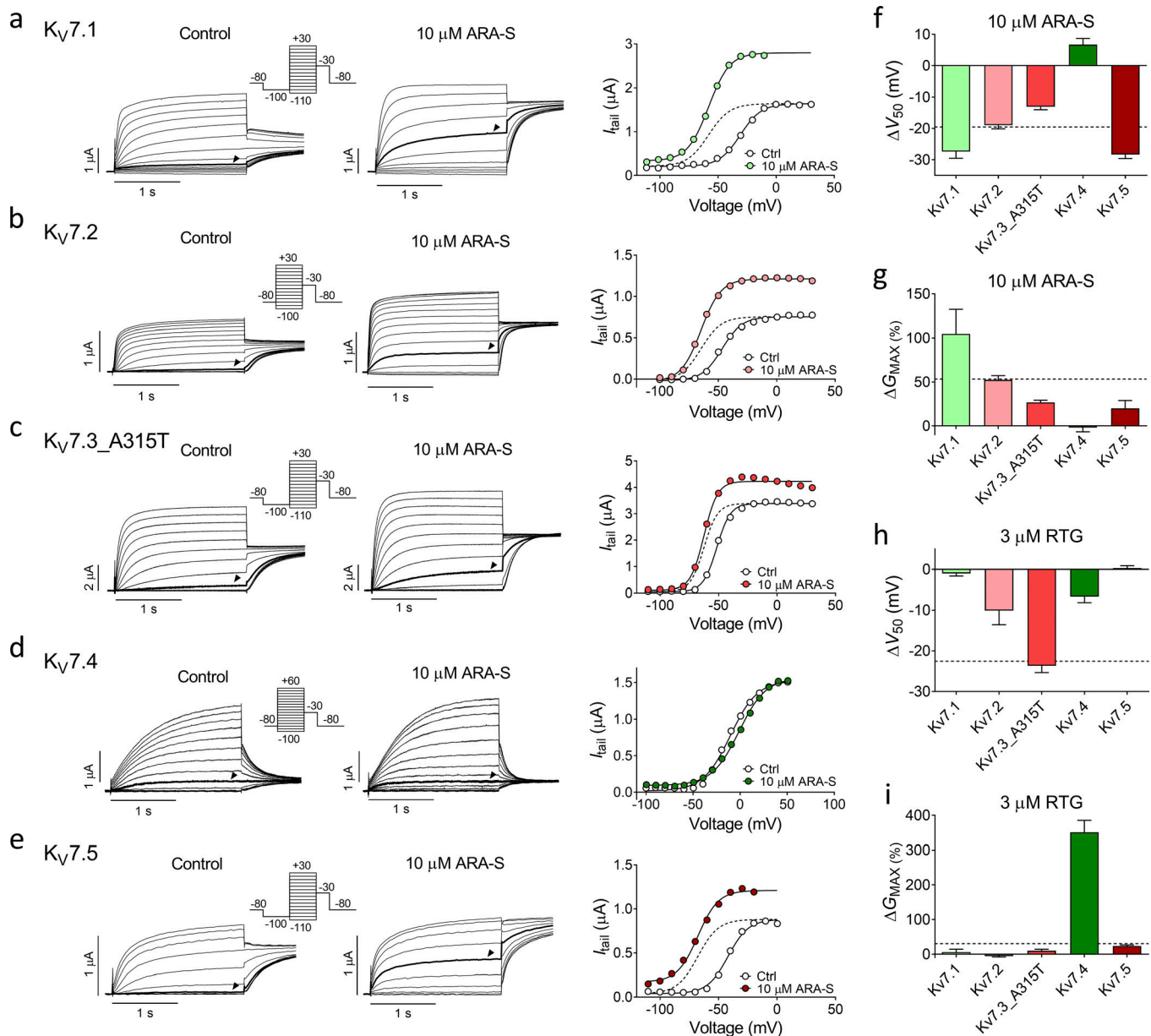
Figure 5. **ARA-S activates all K$_V$7 family members but K$_V$7.4. (a–e)** Representative current traces and corresponding $G(V)$ curves for hK$_V$7.1, hK$_V$7.2, hK$_V$7.3_A315T, hK$_V$7.4, and hK$_V$7.5 before and after application of 10 µM ARA-S. Arrowheads indicate an activating voltage step to −60 mV except for K$_V$7.1 and K$_V$7.4, for which the arrowheads indicate an activating voltage step to −50 mV and −30 mV, respectively. Dashed line in the $G(V)$ curve shows the curve for 10 µM ARA-S normalized to G_{MAX} of control. **(f and g)** Mean shift in V_{50} (f) and increase in G_{MAX} (g) induced by 10 µM ARA-S. Data shown as mean ± SEM; n = 9–13. The effect of ARA-S on G_{MAX} of hK$_V$7.1 and hK$_V$7.5 might be underestimated because of a tendency of decreasing tail currents in the presence of ARA-S at the most positive voltages (e.g., Fig. 5e), the reason for which remains unknown. **(h and i)** Same as in f and g, but for 3 µM retigabine (RTG). n = 4–5. Dashed lines in f–i denote effect of indicated treatment on hK$_V$7.2/3.

coapplication of 1 µM ARA-S and 1 µM retigabine induced a 20-fold increase of the current at −60 mV, compared with a three- to fourfold increase for 1 µM of either of the compounds individually (Fig. 6 d). Notably, the 20-fold increase of the current at −60 mV induced by coapplication is almost three times the increase of the current induced by 10 µM ARA-S alone (compare with Fig. 1 h). Thus, the combined activating effect of low concentrations of ARA-S and retigabine substantially increased the current generated by hK$_V$7.2/3 at voltages corresponding to the resting membrane potential of neurons.

Improved subtype selectivity when combining low concentrations of ARA-S and retigabine

As a second step, we compared the off-target effect of coapplying ARA-S and retigabine on hK$_V$7.1, hK$_V$7.4, hK$_V$7.5, and hK$_V$7.4/5 channels with the effects of the compounds individually. hK$_V$7.4/5 was included in this analysis because heterotetramers of hK$_V$7.4 and hK$_V$7.5 have been implicated in regulation of smooth muscle contraction (Brueggemann et al., 2014; Chadha et al., 2014; Provence et al., 2018). We compared the effect of either 10 µM ARA-S or 3 µM retigabine individually with that of
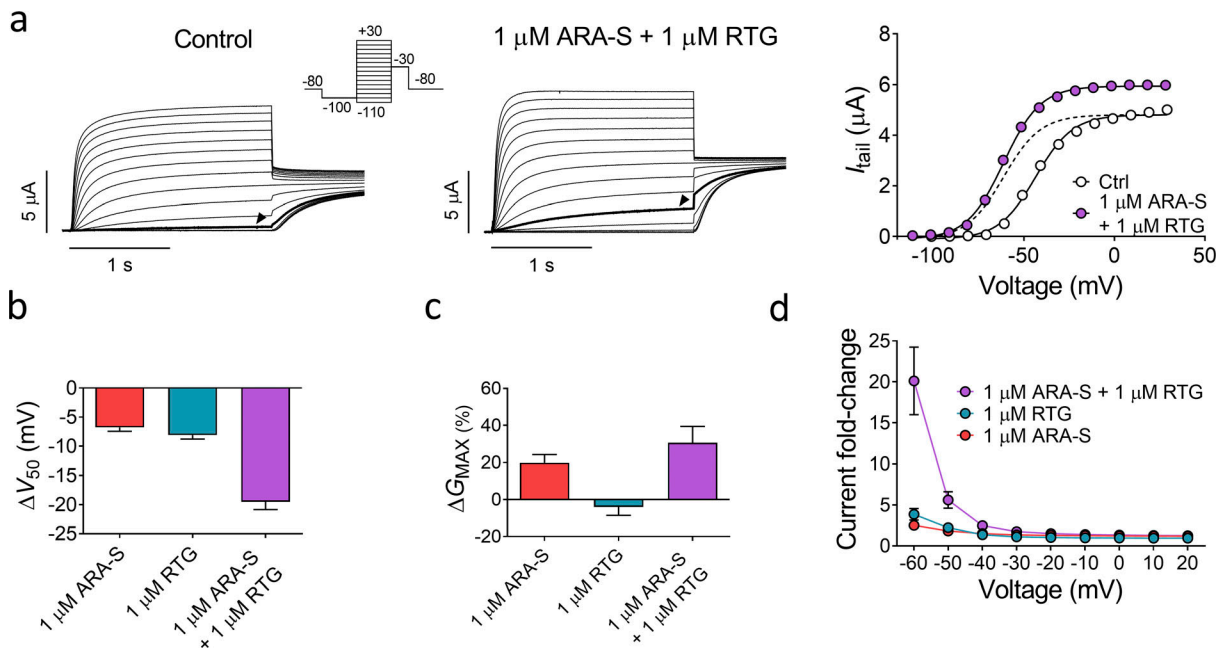
Figure 6. Coapplication of low concentrations of ARA-S and retigabine improves the activating effect on hK$_V$7.2/3. (a) Representative current traces and corresponding $G(V)$ curves for hK$_V$7.2/3 before and after coapplication of 1 μM ARA-S and 1 μM retigabine (RTG). Arrowheads indicate an activating voltage step to −60 mV. Insert of used voltage clamp protocols. Dashed line in the $G(V)$ curve shows the curve for coapplication of 1 μM ARA-S and 1 μM retigabine normalized to G_{MAX} of control. **(b and c)** Mean shift in V_{50} (b) and increase in G_{MAX} (c) of hK$_V$7.2/3 induced by indicated treatment. Data shown as mean ± SEM; n = 7–10. **(d)** Mean hK$_V$7.2/3 current fold increase at different voltages induced by indicated treatment. Data shown as mean ± SEM; n = 7–10.

coapplication of 1 μM ARA-S and 1 μM retigabine, as these three treatments all shifted V_{50} of the hK$_V$7.2/3 channel by about −20 mV (Fig. 7 a). We will refer to these three treatments as ARA-S$_{high}$, retigabine$_{high}$, and coapplication. As was shown in Fig. 5, ARA-S$_{high}$ primarily induced off-target effects on hK$_V$7.1 and hK$_V$7.5 by shifting V_{50} by about −30 mV (Fig. 7 a). ARA-S$_{high}$ induced similar off-target effects on hK$_V$7.4/5 by shifting V_{50} by about −25 mV (Fig. 7 a). Retigabine$_{high}$, on the other hand,

primarily induced off-target effects on hK$_V$7.4 by increasing G_{MAX} by 350% (Fig. 7 b and Fig. S7 a). Retigabine$_{high}$ also induced off-target effects on hK$_V$7.4/5 by increasing G_{MAX} by 180% (Fig. 7 b). In contrast, all off-target effects were reduced during coapplication: coapplication shifted V_{50} of hK$_V$7.1, hK$_V$7.5, and hK$_V$7.4/5 by less than 4 mV (Fig. 7 a and Fig. S7 c) and reduced the increase in G_{MAX} of hK$_V$7.4 and hK$_V$7.4/5 to 75% and 35%, respectively (Fig. 7 b and Fig. S7 b).
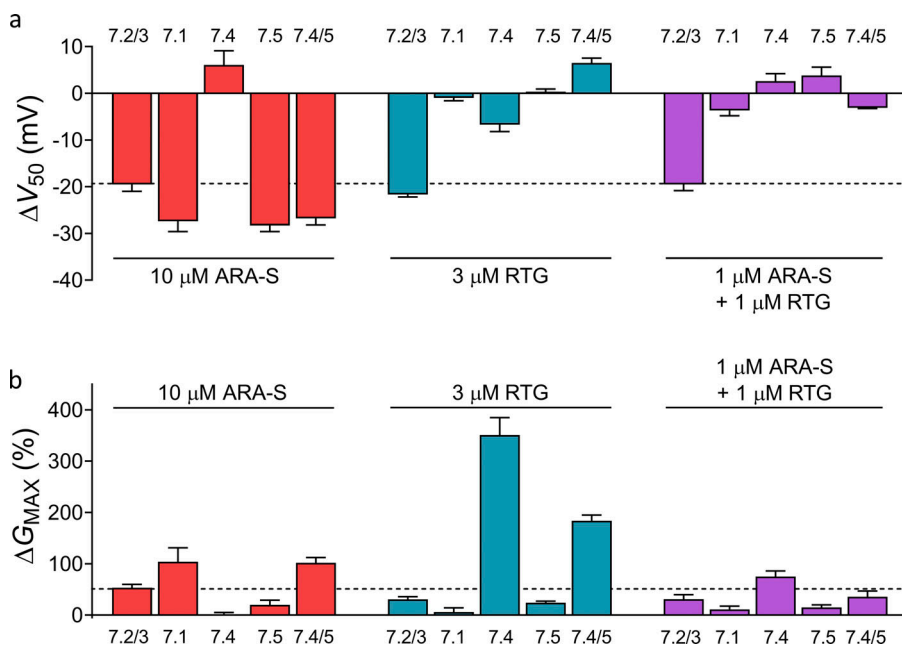

Figure 7. Coapplication of low concentrations of ARA-S and retigabine limits the off-target effect on other hK$_V$7 subtypes. (a) Mean shift in V_{50} induced by 10 μM ARA-S, 3 μM retigabine (RTG), or 1 μM ARA-S + 1 μM retigabine coapplied on indicated channels. Data shown as mean ± SEM; n = 4–13. Dashed line denotes a shift in V_{50} of −20 mV, which was the approximate effect of each treatment on hK$_V$7.2/3. **(b)** Mean increase in G_{MAX} induced by 10 μM ARA-S, 3 μM retigabine, or 1 μM ARA-S + 1 μM retigabine coapplied on indicated channels. Data shown as mean ± SEM; n = 4–13. Dashed line denotes an increase in G_{MAX} of 50%, which was the approximate effect of 10 μM ARA-S on hK$_V$7.2/3.

We also tested the concept of coapplication using ICA73 (structure in Fig. S8 a). Although 20 µM of ICA73 alone (referred to as ICA73$_{high}$) activated hK$_V$7.2/3 by shifting V_{50} by –15 mV (Fig. S8 a), ICA73$_{high}$ also induced off-target effects on hK$_V$7.4 by shifting V_{50} by –15 mV and increasing G_{MAX} by 175% (Fig. S8, a and c). Like ICA73$_{high}$, coapplication of 2 µM ARA-S and 6 µM ICA73 shifted V_{50} of hK$_V$7.2/3 by about –15 mV (Fig. S8 a). However, coapplication did not shift V_{50} of hK$_V$7.4 (P > 0.05 with Student's t test) and reduced the increase in G_{MAX} of hK$_V$7.4 to 66% (Fig. S8, a and c). Altogether, these experiments demonstrate that ARA-S can be combined with either retigabine or ICA73 to preserve the activating effect on the hK$_V$7.2/3 channel and limit off-target effects on other hK$_V$7 subtypes.

Discussion

In this study, we make three important observations. First, we uncover that specific endogenous compounds belonging to the endocannabinoid family activate the hK$_V$7.2/3 channel expressed in *Xenopus* oocytes. ARA-S in particular was identified as a potent hK$_V$7.2/3 activator, which activated the channel by both shifting the voltage dependence of channel opening toward negative voltages and increasing the maximal conductance. Second, we found that ARA-S activates hK$_V$7.2/3 through a different mechanism than retigabine and that these two compounds differ in their hK$_V$7 subtype selectivity. The activating effect of retigabine on hK$_V$7.2/3 has been extensively studied. Retigabine activates hK$_V$7.2/3 by binding to an internal site in the pore domain, in which a tryptophan is critical for binding, to stabilize the open channel (Schenzer et al., 2005; Wuttke et al., 2005; Kim et al., 2015). For endocannabinoids, we here describe that conserved positively charged residues in S4 and S6, distinct from the retigabine site but corresponding to those previously shown to be important for polyunsaturated fatty acid effects in hK$_V$7.1 (Liin et al., 2018), are important for ARA-S–induced activation. We also describe that the negative charge of the endocannabinoid head is critical for the effect on hK$_V$7.2/3, which could explain why 2-AG, AEA, and NADA are ineffective, and that a saturated tail appears to eliminate the effect. Given the corresponding important channel residues identified and the shared chemical properties of polyunsaturated fatty acids and endocannabinoids, we find it likely that endocannabinoids act through a similar mechanism to that previously described for polyunsaturated fatty acids (Liin et al., 2018). Thus, we hypothesize that the negative charge of the endocannabinoid head group is required to enable electrostatic interaction with S4 arginines (to facilitate outward S4 movement) and with the S6 arginine (to induce structural rearrangements in the pore that enhance potassium conductance; Liin et al., 2018). The flexibility of a polyunsaturated tail to adopt bent conformations has been reported to allow intimate and high-affinity interaction of polyunsaturated fatty acids with other voltage-gated ion channels (Tian et al., 2016; Yazdi et al., 2016). Possibly, the more rigid nature of monounsaturated and saturated endocannabinoid tails limits bent conformations needed for interaction with hK$_V$7.2/3. Future studies are needed to further resolve molecular details for endocannabinoid interactions with hK$_V$7.2/3. We note that

the electrostatic nature of the proposed interaction between the negative endocannabinoid head group and positive residues in the channel is reminiscent of the interaction between PIP$_2$ (phosphatidylinositol 4,5-bisphosphate) and K$_V$7 channels (Zaydman and Cui, 2014; Taylor and Sanders, 2017). However, whereas PIP$_2$ interacts with positively charged residues in the inner half of the channel (because PIP$_2$ is localized to the inner leaflet of the plasma membrane), we propose that endocannabinoids primarily act on residues in the outer half of the channel. Third, we demonstrate how to leverage upon the different hK$_V$7 subtype selectivities through coapplication of ARA-S and retigabine for efficient activation of hK$_V$7.2/3 while limiting the off-target effect on hK$_V$7.1, hK$_V$7.4, hK$_V$7.5, and hK$_V$7.4/5. Beneficial effects of coapplication were also achieved by combining ARA-S and ICA73.

Can coapplication of low doses of two compounds targeting the M-channel be a viable approach to reach adequate anti-convulsant effect while reducing adverse effects usually caused by higher doses of these compounds? Manville and Abbott (2018) lend support to efficient anti-convulsant effect in an animal epilepsy model of coadministration of multiple compounds targeting the M-channel. Our experiments on hK$_V$7 channels expressed in *Xenopus* oocytes show that combined application of low concentrations of ARA-S and retigabine effectively activates the M-channel and that strategic combination of M-channel activators with different subtype selectivity limits off-target effects on other hK$_V$7 subtypes. Developing new anti-convulsants is a costly and exhaustive process. Withdrawal of a drug that has passed critical safety testing is a major setback. Our strategy of targeting the M-channel with dual compounds acting through a distinct mechanism, here tested in *Xenopus* oocytes, might offer ways for promising drugs with some degree of off-target effect to be tolerated clinically. Therefore, we encourage further exploration of this concept in more complex experimental systems. Such studies need to address important questions, such as which M-channel activators should ideally be combined (considering critical aspects such as ion channel selectivity, apparent affinity, and efficacy) and the balance between anti-excitable effects in neurons and possible off-target effects in other cell types. Clinical challenges with combined treatment using two or more drugs include possible varying pharmacodynamic profiles of the drugs used and possible drug interaction. However, as ∼20% of patients suffering from epilepsy are treated using two or more drugs (Brodie et al., 2012), these are challenges already faced by current treatment strategies.

We note that coapplication of 1 µM ARA-S and 1 µM retigabine induced hK$_V$7.2/3 effects that were slightly larger than expected from additive effects (Fig. 6, b–d). In particular, the increase of current amplitude at –60 mV was unexpectedly large upon coapplication (Fig. 6 d). Manville and Abbott (2018) described synergistic effects on hK$_V$7.2/3 upon coapplication of retigabine and herbal extracts. They proposed that the ability of such compounds to simultaneously occupy a shared binding pocket in combination with prominent effects on different subunits in the hK$_V$7.2/3 channel (hK$_V$7.3 for retigabine and hK$_V$7.2 for herbal components) underlies synergistic effects

(Manville and Abbott, 2018). We observed larger ARA-S effects on hK$_V$7.2 than on hK$_V$7.3. However, because ARA-S and retigabine use different binding sites, it is not clear if different preference for different hK$_V$7.2/3 subunits contributed to the apparent synergy in ARA-S and retigabine effects. Alternatively, presence of one of the compounds may facilitate action of the other compound (e.g., by improving affinity or efficacy). However, at this point, we are careful with interpretation of additive versus synergistic effects in our data, as the most prominent indication of synergy was observed for current amplitudes at −60 mV, which is at the foot of the $G(V)$ curve, meaning that small variations in V_{50} between cells may impact the magnitude of current increase. Further characterization of additive/synergistic effects and possible underlying mechanisms is worth exploring in future studies.

Because ARA-S is an endogenous compound, this raises several questions. For example, does ARA-S have physiological or pathophysiological effects in the body at the concentrations used in this study, and could these effects be tuned by regulating the concentration of ARA-S? Although all five arachidonic acid–based endocannabinoids studied in this work have been detected in neuronal tissue from mammals (Devane et al., 1992; Kondo et al., 1998; Bisogno et al., 2000; Huang et al., 2001; Milman et al., 2006), the understanding of the endogenous functions of some of them is less clear. The endocannabinoids 2-AG and AEA have been shown to signal noncanonically through other pathways than cannabinoid receptors (Bondarenko et al., 2017; Gantz and Bean, 2017). ARA-S has been isolated from bovine brain (Milman et al., 2006), but it is not known if ARA-S is present in human tissue and, if so, at what concentrations. This makes it difficult to evaluate whether ARA-S might have physiological or pathophysiological functions in the human body. Future studies will hopefully shed light on whether ARA-S endogenously reaches concentrations triggering noncanonical signaling through interaction with ion channels such as hK$_V$7.2/3, the BK channel (Godlewski et al., 2009), and the N-type Ca$_V$ channel (Guo et al., 2008).

To conclude, this study shows that specific members within the endocannabinoid family, most notably ARA-S, target and activate the neuronal M-channel. The pronounced activation of the M-channel by low concentrations of ARA-S highlights ARA-S as an interesting model compound for future development of new treatment strategies for epilepsy targeting the M-channel. The successful combination of ARA-S and retigabine (as well as ARA-S and ICA73) to achieve M-channel activation with improved hK$_V$7 subtype selectivity allows for possibilities to use such ARA-S mimetic compounds either alone or in conjunction with other M-channel activators. Future studies are required to study the concept of combined treatment in more complex systems.

Acknowledgments

References

Abdel-Magid, A.F.. 2015. Allosteric modulators: an emerging concept in drug discovery. *ACS Med. Chem. Lett.* 6:104–107. https://doi.org/10.1021/ml5005365

Bisogno, T., D. Melck, N.M. Bobrov MYu, N.M. Gretskaya, V.V. Bezuglov, L. De Petrocellis, and V. Di Marzo. 2000. N-acyl-dopamines: novel synthetic CB(1) cannabinoid-receptor ligands and inhibitors of anandamide inactivation with cannabimimetic activity in vitro and in vivo. *Biochem. J.* 351:817–824. https://doi.org/10.1042/bj3510817

Bohannon, B.M., M.E. Perez, S.I. Liin, and H.P. Larsson. 2019. ω-6 and ω-9 polyunsaturated fatty acids with double bonds near the carboxyl head have the highest affinity and largest effects on the cardiac I$_{Ks}$ potassium channel. *Acta Physiol. (Oxf.).* 225. e13186. https://doi.org/10.1111/apha.13186

Bohannon, B.M., X. Wu, X. Wu, M.E. Perez, S.I. Liin, and H.P. Larsson. 2020. Polyunsaturated fatty acids produce a range of activators for heterogeneous IKs channel dysfunction. *J. Gen. Physiol.* 152. e201912396. https://doi.org/10.1085/jgp.201912396

Bojesen, I.N., and H.S. Hansen. 2003. Binding of anandamide to bovine serum albumin. *J. Lipid Res.* 44:1790–1794. https://doi.org/10.1194/jlr.M300170-JLR200

Bondarenko, A.I., O. Panasiuk, I. Okhai, F. Montecucco, K.J. Brandt, and F. Mach. 2017. Direct activation of Ca^{2+} and voltage-gated potassium channels of large conductance by anandamide in endothelial cells does not support the presence of endothelial atypical cannabinoid receptor. *Eur. J. Pharmacol.* 805:14–24. https://doi.org/10.1016/j.ejphar.2017.03.038

Börjesson, S.I., and F. Elinder. 2011. An electrostatic potassium channel opener targeting the final voltage sensor transition. *J. Gen. Physiol.* 137: 563–577. https://doi.org/10.1085/jgp.201110599

Börjesson, S.I., S. Hammarström, and F. Elinder. 2008. Lipoelectric modification of ion channel voltage gating by polyunsaturated fatty acids. *Biophys. J.* 95:2242–2253. https://doi.org/10.1529/biophysj.108.130757

Brodie, M.J., H. Lerche, A. Gil-Nagel, C. Elger, S. Hall, P. Shin, V. Nohria, and H. Mansbach; RESTORE 2 Study Group. 2010. Efficacy and safety of adjunctive ezogabine (retigabine) in refractory partial epilepsy. *Neurology.* 75:1817–1824. https://doi.org/10.1212/WNL.0b013e3181fd6170

Brodie, M.J., S.J. Barry, G.A. Bamagous, J.D. Norrie, and P. Kwan. 2012. Patterns of treatment response in newly diagnosed epilepsy. *Neurology.* 78: 1548–1554. https://doi.org/10.1212/WNL.0b013e3182563b19

Brueggemann, L.I., A.R. Mackie, L.L. Cribbs, J. Freda, A. Tripathi, M. Majetschak, and K.L. Byron. 2014. Differential protein kinase C-dependent modulation of Kv7.4 and Kv7.5 subunits of vascular Kv7 channels. *J. Biol. Chem.* 289:2099–2111. https://doi.org/10.1074/jbc.M113.527820

Chadha, P.S., T.A. Jepps, G. Carr, J.B. Stott, H.L. Zhu, W.C. Cole, and I.A. Greenwood. 2014. Contribution of kv7.4/kv7.5 heteromers to intrinsic and calcitonin gene-related peptide-induced cerebral reactivity. *Arterioscler. Thromb. Vasc. Biol.* 34:887–893. https://doi.org/10.1161/ATVBAHA.114.303405

Changeux, J.P., and A. Christopoulos. 2016. Allosteric Modulation as a Unifying Mechanism for Receptor Function and Regulation. *Cell.* 166:1084–1102. https://doi.org/10.1016/j.cell.2016.08.015

Choveau, F.S., S.M. Bierbower, and M.S. Shapiro. 2012a. Pore helix-S6 interactions are critical in governing current amplitudes of KCNQ3 K+ channels. *Biophys. J.* 102:2499–2509. https://doi.org/10.1016/j.bpj.2012.04.019

Choveau, F.S., C.C. Hernandez, S.M. Bierbower, and M.S. Shapiro. 2012b. Pore determinants of KCNQ3 K+ current expression. *Biophys. J.* 102:2489–2498. https://doi.org/10.1016/j.bpj.2012.04.018

Devane, W.A., L. Hanus, A. Breuer, R.G. Pertwee, L.A. Stevenson, G. Griffin, D. Gibson, A. Mandelbaum, A. Etinger, and R. Mechoulam. 1992. Isolation and structure of a brain constituent that binds to the cannabinoid receptor. *Science.* 258:1946–1949. https://doi.org/10.1126/science.1470919

Di Marzo, V., M. Bifulco, and L. De Petrocellis. 2004. The endocannabinoid system and its therapeutic exploitation. *Nat. Rev. Drug Discov.* 3:771–784. https://doi.org/10.1038/nrd1495

Elinder, F., and S.I. Liin. 2017. Actions and Mechanisms of Polyunsaturated Fatty Acids on Voltage-Gated Ion Channels. *Front. Physiol.* 8:43. https://doi.org/10.3389/fphys.2017.00043

Foster, D.J., and P.J. Conn. 2017. Allosteric Modulation of GPCRs: New Insights and Potential Utility for Treatment of Schizophrenia and Other CNS Disorders. *Neuron.* 94:431–446. https://doi.org/10.1016/j.neuron.2017.03.016

French, J.A., B.W. Abou-Khalil, R.F. Leroy, E.M. Yacubian, P. Shin, S. Hall, H. Mansbach, and V. Nohria; RESTORE 1/Study 301 Investigators. 2011. Randomized, double-blind, placebo-controlled trial of ezogabine (retigabine) in partial epilepsy. *Neurology.* 76:1555–1563. https://doi.org/10.1212/WNL.0b013e3182194bd3

Gantz, S.C., and B.P. Bean. 2017. Cell-Autonomous Excitation of Midbrain Dopamine Neurons by Endocannabinoid-Dependent Lipid Signaling. *Neuron.* 93:1375–1387.e2. https://doi.org/10.1016/j.neuron.2017.02.025

Garin Shkolnik, T., H. Feuerman, E. Didkovsky, I. Kaplan, R. Bergman, L. Pavlovsky, and E. Hodak. 2014. Blue-gray mucocutaneous discoloration: a new adverse effect of ezogabine. *JAMA Dermatol.* 150:984–989. https://doi.org/10.1001/jamadermatol.2013.8895

Godlewski, G., L. Offertáler, D. Osei-Hyiaman, F.M. Mo, J. Harvey-White, J. Liu, M.I. Davis, L. Zhang, R.K. Razdan, G. Milman, et al. 2009. The endocannabinoid brain constituent N-arachidonoyl L-serine is an activator of large conductance Ca2+-activated K+ channels. *J. Pharmacol. Exp. Ther.* 328:351–361. https://doi.org/10.1124/jpet.108.144717

Gómez-Posada, J.C., A. Etxeberría, M. Roura-Ferrer, P. Areso, M. Masin, R.D. Murrell-Lagnado, and A. Villarroel. 2010. A pore residue of the KCNQ3 potassium M-channel subunit controls surface expression. *J. Neurosci.* 30:9316–9323. https://doi.org/10.1523/JNEUROSCI.0851-10.2010

Groseclose, M.R., and S. Castellino. 2019. An Investigation into Retigabine (Ezogabine) Associated Dyspigmentation in Rat Eyes by MALDI Imaging Mass Spectrometry. *Chem. Res. Toxicol.* 32:294–303. https://doi.org/10.1021/acs.chemrestox.8b00313

Gunthorpe, M.J., C.H. Large, and R. Sankar. 2012. The mechanism of action of retigabine (ezogabine), a first-in-class K+ channel opener for the treatment of epilepsy. *Epilepsia.* 53:412–424. https://doi.org/10.1111/j.1528-1167.2011.03365.x

Guo, J., D.J. Williams, and S.R. Ikeda. 2008. N-arachidonoyl L-serine, a putative endocannabinoid, alters the activation of N-type Ca2+ channels in sympathetic neurons. *J. Neurophysiol.* 100:1147–1151. https://doi.org/10.1152/jn.01204.2007

Hempel, R., H. Schupke, P.J. McNeilly, K. Heinecke, C. Kronbach, C. Grunwald, G. Zimmermann, C. Griesinger, J. Engel, and T. Kronbach. 1999. Metabolism of retigabine (D-23129), a novel anticonvulsant. *Drug Metab. Dispos.* 27:613–622.

Holt, J.R., E.A. Stauffer, D. Abraham, and G.S. Géléoc. 2007. Dominant-negative inhibition of M-like potassium conductances in hair cells of the mouse inner ear. *J. Neurosci.* 27:8940–8951. https://doi.org/10.1523/JNEUROSCI.2085-07.2007

Huang, S.M., T. Bisogno, T.J. Petros, S.Y. Chang, P.A. Zavitsanos, R.E. Zipkin, R. Sivakumar, A. Coop, D.Y. Maeda, L. De Petrocellis, et al. 2001. Identification of a new class of molecules, the arachidonyl amino acids, and characterization of one member that inhibits pain. *J. Biol. Chem.* 276:42639–42644. https://doi.org/10.1074/jbc.M107351200

Kim, R.Y., M.C. Yau, J.D. Galpin, G. Seebohm, C.A. Ahern, S.A. Pless, and H.T. Kurata. 2015. Atomic basis for therapeutic activation of neuronal potassium channels. *Nat. Commun.* 6:8116. https://doi.org/10.1038/ncomms9116

Kondo, S., H. Kondo, S. Nakane, T. Kodaka, A. Tokumura, K. Waku, and T. Sugiura. 1998. 2-Arachidonoylglycerol, an endogenous cannabinoid receptor agonist: identification as one of the major species of monoacylglycerols in various rat tissues, and evidence for its generation through CA2+-dependent and -independent mechanisms. *FEBS Lett.* 429:152–156. https://doi.org/10.1016/S0014-5793(98)00581-X

Kumar, M., N. Reed, R. Liu, E. Aizenman, P. Wipf, and T. Tzounopoulos. 2016. Synthesis and Evaluation of Potent KCNQ2/3-Specific Channel Activators. *Mol. Pharmacol.* 89:667–677. https://doi.org/10.1124/mol.115.103200

Liin, S.I., M. Silverå Ejneby, R. Barro-Soria, M.A. Skarsfeldt, J.E. Larsson, F. Starck Härlin, T. Parkkari, B.H. Bentzen, N. Schmitt, H.P. Larsson, et al. 2015. Polyunsaturated fatty acid analogs act antiarrhythmically on the cardiac IKs channel. *Proc. Natl. Acad. Sci. USA.* 112:5714–5719. https://doi.org/10.1073/pnas.1503488112

Liin, S.I., U. Karlsson, B.H. Bentzen, N. Schmitt, and F. Elinder. 2016. Polyunsaturated fatty acids are potent openers of human M-channels expressed in Xenopus laevis oocytes. *Acta Physiol. (Oxf.).* 218:28–37.

Liin, S.I., S. Yazdi, R. Ramentol, R. Barro-Soria, and H.P. Larsson. 2018. Mechanisms Underlying the Dual Effect of Polyunsaturated Fatty Acid Analogs on Kv7.1. *Cell Rep.* 24:2908–2918. https://doi.org/10.1016/j.celrep.2018.08.031

Łuszczki, J.J.. 2009. Third-generation antiepileptic drugs: mechanisms of action, pharmacokinetics and interactions. *Pharmacol. Rep.* 61:197–216. https://doi.org/10.1016/S1734-1140(09)70024-6

Main, M.J., J.E. Cryan, J.R. Dupere, B. Cox, J.J. Clare, and S.A. Burbidge. 2000. Modulation of KCNQ2/3 potassium channels by the novel anticonvulsant retigabine. *Mol. Pharmacol.* 58:253–262. https://doi.org/10.1124/mol.58.2.253

Manville, R.W., and G.W. Abbott. 2018. Ancient and modern anticonvulsants act synergistically in a KCNQ potassium channel binding pocket. *Nat. Commun.* 9:3845. https://doi.org/10.1038/s41467-018-06339-2

Mechoulam, R., S. Ben-Shabat, L. Hanus, M. Ligumsky, N.E. Kaminski, A.R. Schatz, A. Gopher, S. Almog, B.R. Martin, D.R. Compton, et al. 1995. Identification of an endogenous 2-monoglyceride, present in canine gut, that binds to cannabinoid receptors. *Biochem. Pharmacol.* 50:83–90. https://doi.org/10.1016/0006-2952(95)00109-D

Miceli, F., M.V. Soldovieri, C.C. Hernandez, M.S. Shapiro, L. Annunziato, and M. Taglialatela. 2008. Gating consequences of charge neutralization of arginine residues in the S4 segment of K(v)7.2, an epilepsy-linked K+ channel subunit. *Biophys. J.* 95:2254–2264. https://doi.org/10.1529/biophysj.107.128371

Milman, G., Y. Maor, S. Abu-Lafi, M. Horowitz, R. Gallily, S. Batkai, F.M. Mo, L. Offertaler, P. Pacher, G. Kunos, et al. 2006. N-arachidonoyl L-serine, an endocannabinoid-like brain constituent with vasodilatory properties. *Proc. Natl. Acad. Sci. USA.* 103:2428–2433. https://doi.org/10.1073/pnas.0510676103

Panaghie, G., and G.W. Abbott. 2007. The role of S4 charges in voltage-dependent and voltage-independent KCNQ1 potassium channel complexes. *J. Gen. Physiol.* 129:121–133. https://doi.org/10.1085/jgp.200609612

Provence, A., D. Angoli, and G.V. Petkov. 2018. Kv7 Channel Pharmacological Activation by the Novel Activator ML213: Role for Heteromeric Kv7.4/Kv7.5 Channels in Guinea Pig Detrusor Smooth Muscle Function. *J. Pharmacol. Exp. Ther.* 364:131–144. https://doi.org/10.1124/jpet.117.243162

Robbins, J.. 2001. KCNQ potassium channels: physiology, pathophysiology, and pharmacology. *Pharmacol. Ther.* 90:1–19. https://doi.org/10.1016/S0163-7258(01)00116-4

Rode, F., J. Svalø, M. Sheykhzade, and L.C. Rønn. 2010. Functional effects of the KCNQ modulators retigabine and XE991 in the rat urinary bladder. *Eur. J. Pharmacol.* 638:121–127. https://doi.org/10.1016/j.ejphar.2010.03.050

Rostock, A., C. Tober, C. Rundfeldt, R. Bartsch, J. Engel, E.E. Polymeropoulos, B. Kutscher, W. Löscher, D. Hönack, H.S. White, et al. 1996. D-23129: a new anticonvulsant with a broad spectrum activity in animal models of epileptic seizures. *Epilepsy Res.* 23:211–223. https://doi.org/10.1016/0920-1211(95)00101-8

Rundfeldt, C.. 1997. The new anticonvulsant retigabine (D-23129) acts as an opener of K+ channels in neuronal cells. *Eur. J. Pharmacol.* 336:243–249. https://doi.org/10.1016/S0014-2999(97)01249-1

Schenzer, A., T. Friedrich, M. Pusch, P. Saftig, T.J. Jentsch, J. Grötzinger, and M. Schwake. 2005. Molecular determinants of KCNQ (Kv7) K+ channel sensitivity to the anticonvulsant retigabine. *J. Neurosci.* 25:5051–5060. https://doi.org/10.1523/JNEUROSCI.0128-05.2005

Shah, M., M. Mistry, S.J. Marsh, D.A. Brown, and P. Delmas. 2002. Molecular correlates of the M-current in cultured rat hippocampal neurons. *J. Physiol.* 544:29–37. https://doi.org/10.1113/jphysiol.2002.028571

Silverå Ejneby, M., X. Wu, N.E. Ottosson, E.P. Münger, I. Lundström, P. Konradsson, and F. Elinder. 2018. Atom-by-atom tuning of the electrostatic potassium-channel modulator dehydroabietic acid. *J. Gen. Physiol.* 150:731–750. https://doi.org/10.1085/jgp.201711965

Splinter, M.Y.. 2012. Ezogabine (retigabine) and its role in the treatment of partial-onset seizures: a review. *Clin. Ther.* 34:1845–56.e1. https://doi.org/10.1016/j.clinthera.2012.07.009

Tatulian, L., P. Delmas, F.C. Abogadie, and D.A. Brown. 2001. Activation of expressed KCNQ potassium currents and native neuronal M-type potassium currents by the anti-convulsant drug retigabine. *J. Neurosci.* 21:5535–5545. https://doi.org/10.1523/JNEUROSCI.21-15-05535.2001

Taylor, K.C., and C.R. Sanders. 2017. Regulation of KCNQ/Kv7 family voltage-gated K^+ channels by lipids. *Biochim. Biophys. Acta Biomembr.* 1859:586–597. https://doi.org/10.1016/j.bbamem.2016.10.023

Tian, Y., M. Aursnes, T.V. Hansen, J.E. Tungen, J.D. Galpin, L. Leisle, C.A. Ahern, R. Xu, S.H. Heinemann, and T. Hoshi. 2016. Atomic determinants of BK channel activation by polyunsaturated fatty acids. *Proc. Natl. Acad. Sci. USA.* 113:13905–13910. https://doi.org/10.1073/pnas.1615562113

Tykocki, N.R., T.J. Heppner, T. Dalsgaard, A.D. Bonev, and M.T. Nelson. 2019. The K_V 7 channel activator retigabine suppresses mouse urinary bladder afferent nerve activity without affecting detrusor smooth muscle K^+ channel currents. *J. Physiol.* 597:935–950. https://doi.org/10.1113/JP277021

Wang, H.S., Z. Pan, W. Shi, B.S. Brown, R.S. Wymore, I.S. Cohen, J.E. Dixon, and D. McKinnon. 1998. KCNQ2 and KCNQ3 potassium channel subunits: molecular correlates of the M-channel. *Science.* 282:1890–1893. https://doi.org/10.1126/science.282.5395.1890

Wang, A.W., R. Yang, and H.T. Kurata. 2017. Sequence determinants of subtype-specific actions of KCNQ channel openers. *J. Physiol.* 595:663–676. https://doi.org/10.1113/JP272762

Wang, C.K., S.M. Lamothe, A.W. Wang, R.Y. Yang, and H.T. Kurata. 2018. Pore- and voltage sensor-targeted KCNQ openers have distinct state-dependent actions. *J. Gen. Physiol.* 150:1722–1734. https://doi.org/10.1085/jgp.201812070

Wu, D., H. Pan, K. Delaloye, and J. Cui. 2010. KCNE1 remodels the voltage sensor of Kv7.1 to modulate channel function. *Biophys. J.* 99:3599–3608. https://doi.org/10.1016/j.bpj.2010.10.018

Wuttke, T.V., G. Seebohm, S. Bail, S. Maljevic, and H. Lerche. 2005. The new anticonvulsant retigabine favors voltage-dependent opening of the Kv7.2 (KCNQ2) channel by binding to its activation gate. *Mol. Pharmacol.* 67:1009–1017. https://doi.org/10.1124/mol.104.010793

Xu, T., L. Nie, Y. Zhang, J. Mo, W. Feng, D. Wei, E. Petrov, L.E. Calisto, B. Kachar, K.W. Beisel, et al. 2007. Roles of alternative splicing in the functional properties of inner ear-specific KCNQ4 channels. *J. Biol. Chem.* 282:23899–23909. https://doi.org/10.1074/jbc.M702108200

Yazdi, S., M. Stein, F. Elinder, M. Andersson, and E. Lindahl. 2016. The Molecular Basis of Polyunsaturated Fatty Acid Interactions with the Shaker Voltage-Gated Potassium Channel. *PLOS Comput. Biol.* 12. e1004704. https://doi.org/10.1371/journal.pcbi.1004704

Zaydman, M.A., and J. Cui. 2014. PIP2 regulation of KCNQ channels: biophysical and molecular mechanisms for lipid modulation of voltage-dependent gating. *Front. Physiol.* 5:195. https://doi.org/10.3389/fphys.2014.00195

Zhang, X., D. Yang, and B.A. Hughes. 2011. KCNQ5/K(v)7.5 potassium channel expression and subcellular localization in primate retinal pigment epithelium and neural retina. *Am. J. Physiol. Cell Physiol.* 301:C1017–C1026. https://doi.org/10.1152/ajpcell.00185.2011
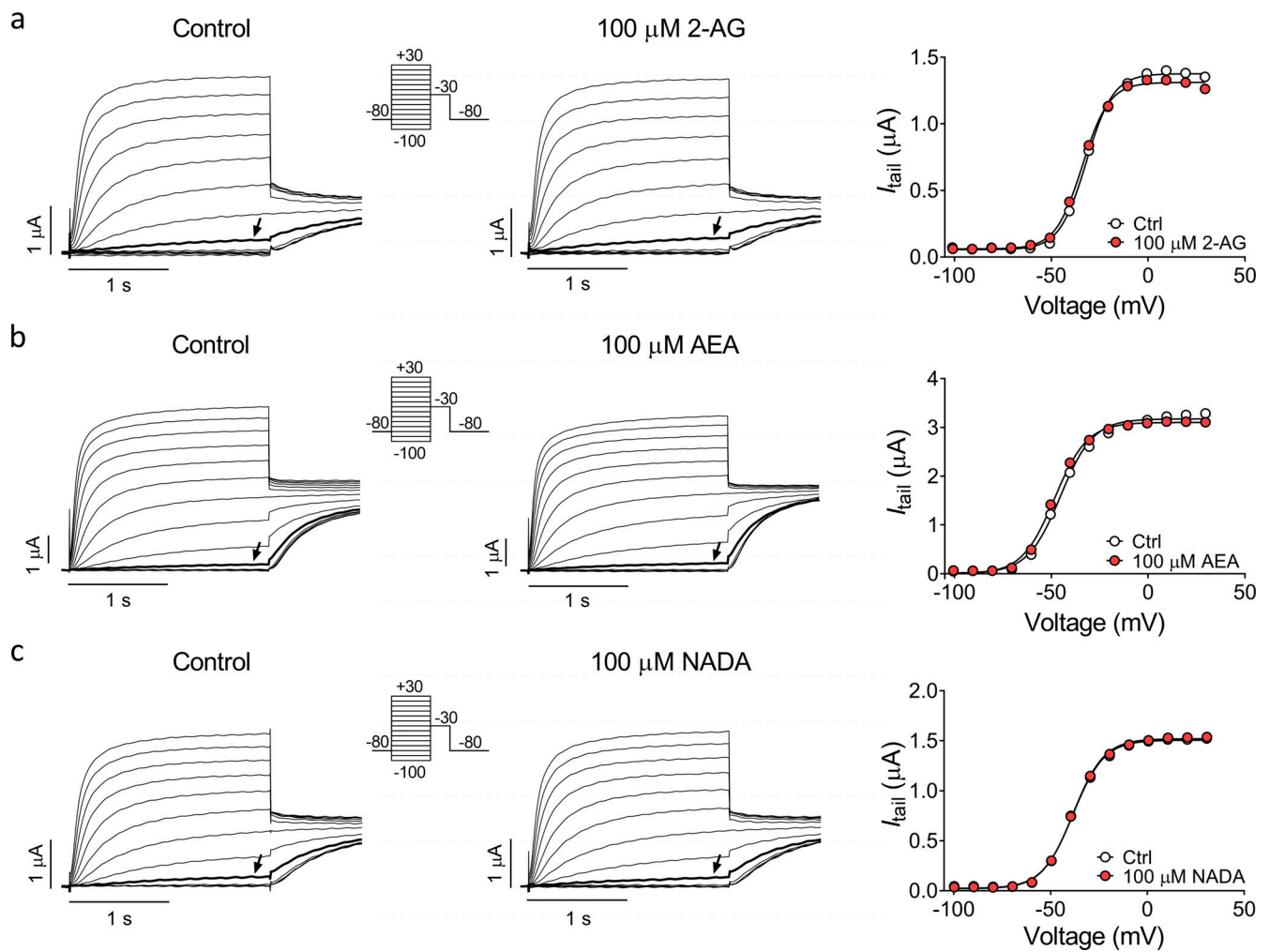
Figure S1. **Specific endocannabinoids do not activate the hK$_V$7.2/3 channel. (a–c)** Representative current traces and corresponding $G(V)$ curves for hK$_V$7.2/3 before and after application of 100 μM indicated endocannabinoids. Arrows indicate an activating voltage step to −40, −60, and −50 mV, respectively. Insert of used voltage clamp protocol.
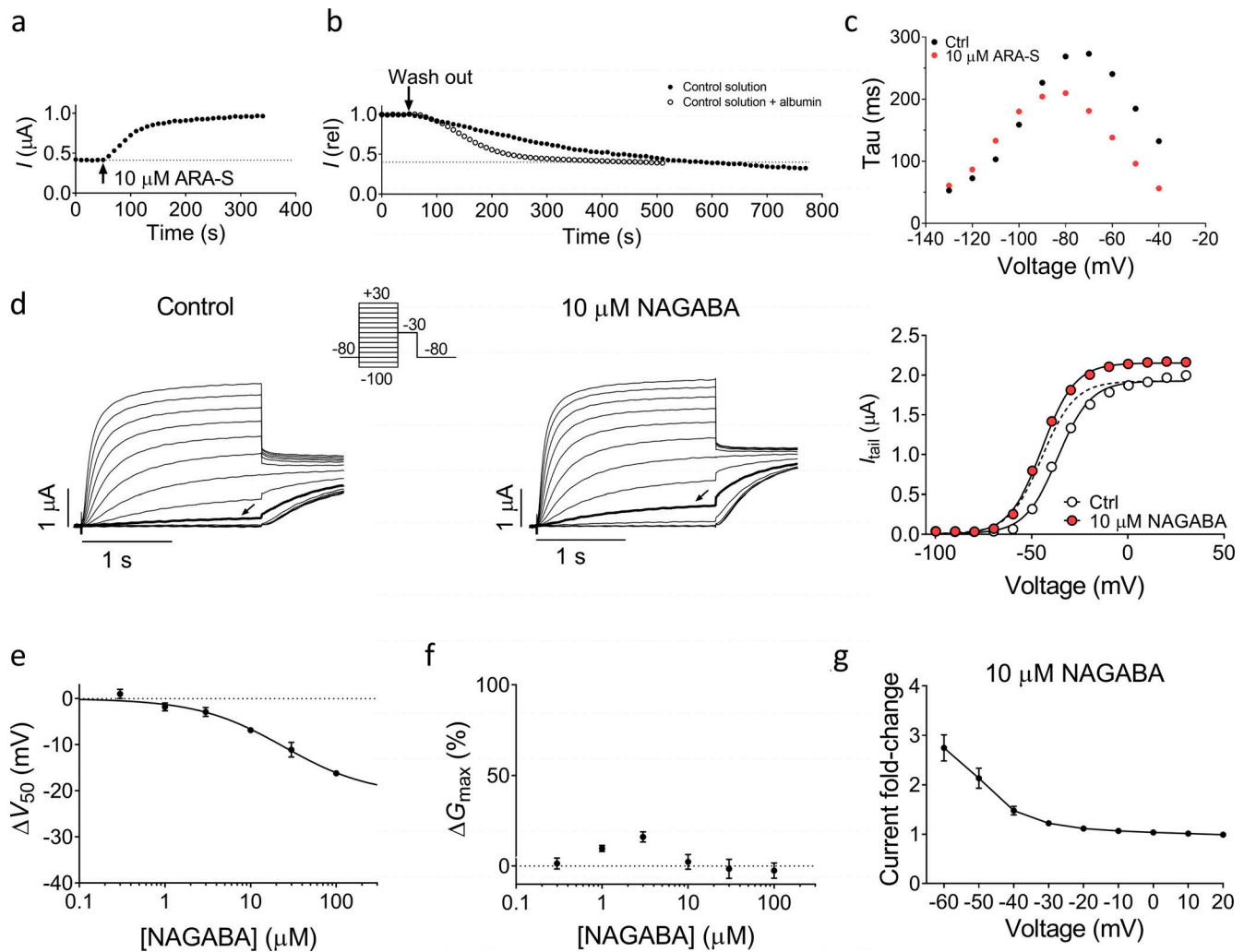
Figure S2. **Effect of ARA-S and NAGABA on hK$_V$7.2/3. (a and b)** Representative example of the wash-in (a) and washout (b) of 10 µM ARA-S with and without supplement of 100 mg/l BSA on hK$_V$7.2/3. The peak current after a 2-s depolarizing step to −40 mV is plotted. Dashed lines indicate basal current level before application of ARA-S. **(c)** Representative effect of 10 µM ARA-S on the kinetics of hK$_V$7.2/3. Data acquired in high K$^+$ solution (100 mM K$^+$) by activating the channel to +20 mV followed by deactivating pulses from −40 to −130 mV in 10-mV steps. τ, determined by fitting a single exponential to the current generated by the deactivation pulse, was plotted toward the voltage of the deactivation pulse. **(d)** Representative current traces and corresponding $G(V)$ curves for hK$_V$7.2/3 before and after application of 10 µM NAGABA. Arrows indicate an activating voltage step to −50 mV. Dashed line shows the curve for 10 µM NAGABA normalized to G_{MAX} of control. Insert of used voltage clamp protocol. **(e)** Concentration-response relation for NAGABA effect on V_{50}. Data shown as mean ± SEM; n = 4–7. $\Delta V_{50:MAX}$ (maximal shift in $V50$) = −21 mV; EC$_{50}$ = 24 µM. **(f)** Concentration-response relation for NAGABA effect on G_{MAX}. Data shown as mean ± SEM; n = 3–7. Concentration-response curve could not be converged. **(g)** Mean hK$_V$7.2/3 current fold increase at different voltages induced by 10 µM NAGABA. Data shown as mean ± SEM; n = 7.
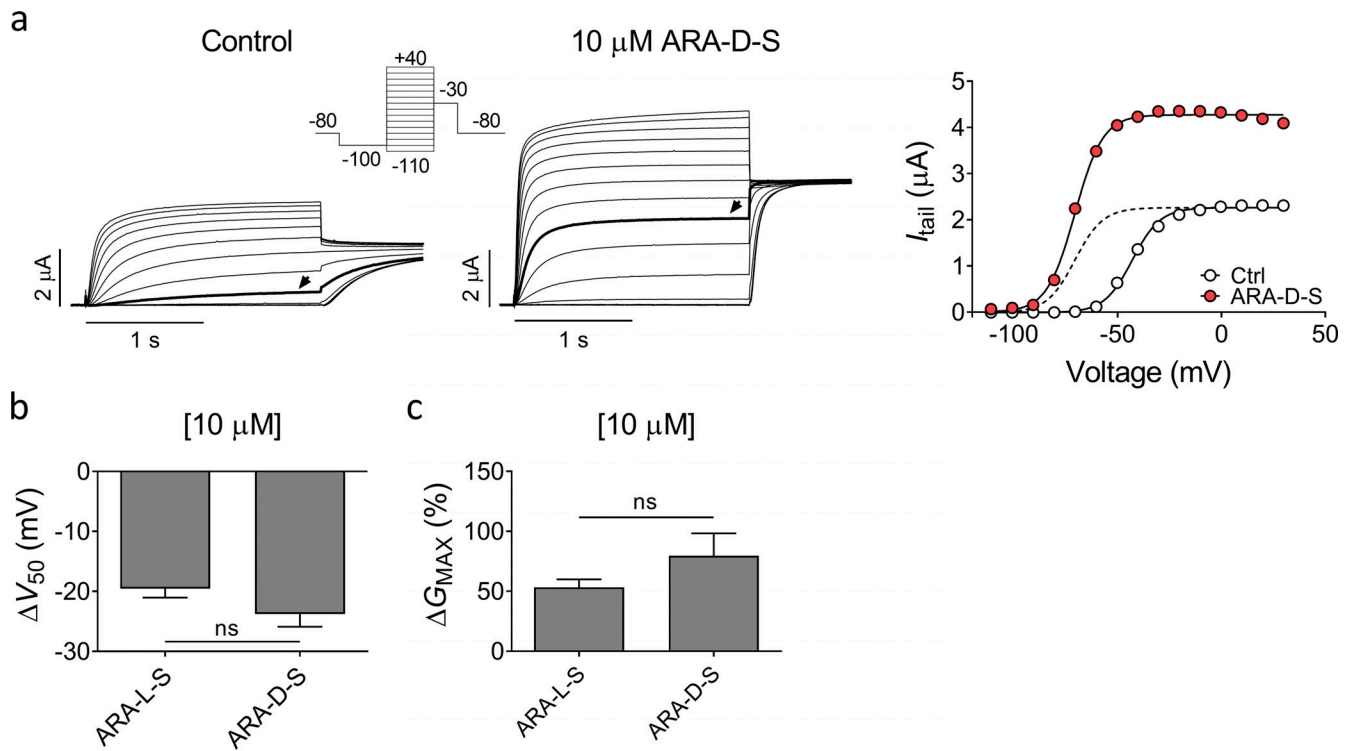
Figure S3. **Effect of N-arachidonoyl-D-serine on hK$_V$7.2/3. (a)** Representative current traces and corresponding $G(V)$ curve of hK$_V$7.2/3 before and after application of 10 μM N-arachidonoyl-D-serine (ARA-D-S). Arrows in the current families indicate an activating voltage step to −50 mV. Insert of used voltage clamp protocol. Dashed line in the $G(V)$ curve shows the curve for 10 μM ARA-D-S normalized to G_{MAX} of control. **(b and c)** Mean shift in V_{50} (b) and increase of G_{MAX} (c) induced by 10 μM ARA-S or 10 μM ARA-D-S on hK$_V$7.2/3. Data shown as mean ± SEM; n = 5–8. Statistics denote Student's t test.
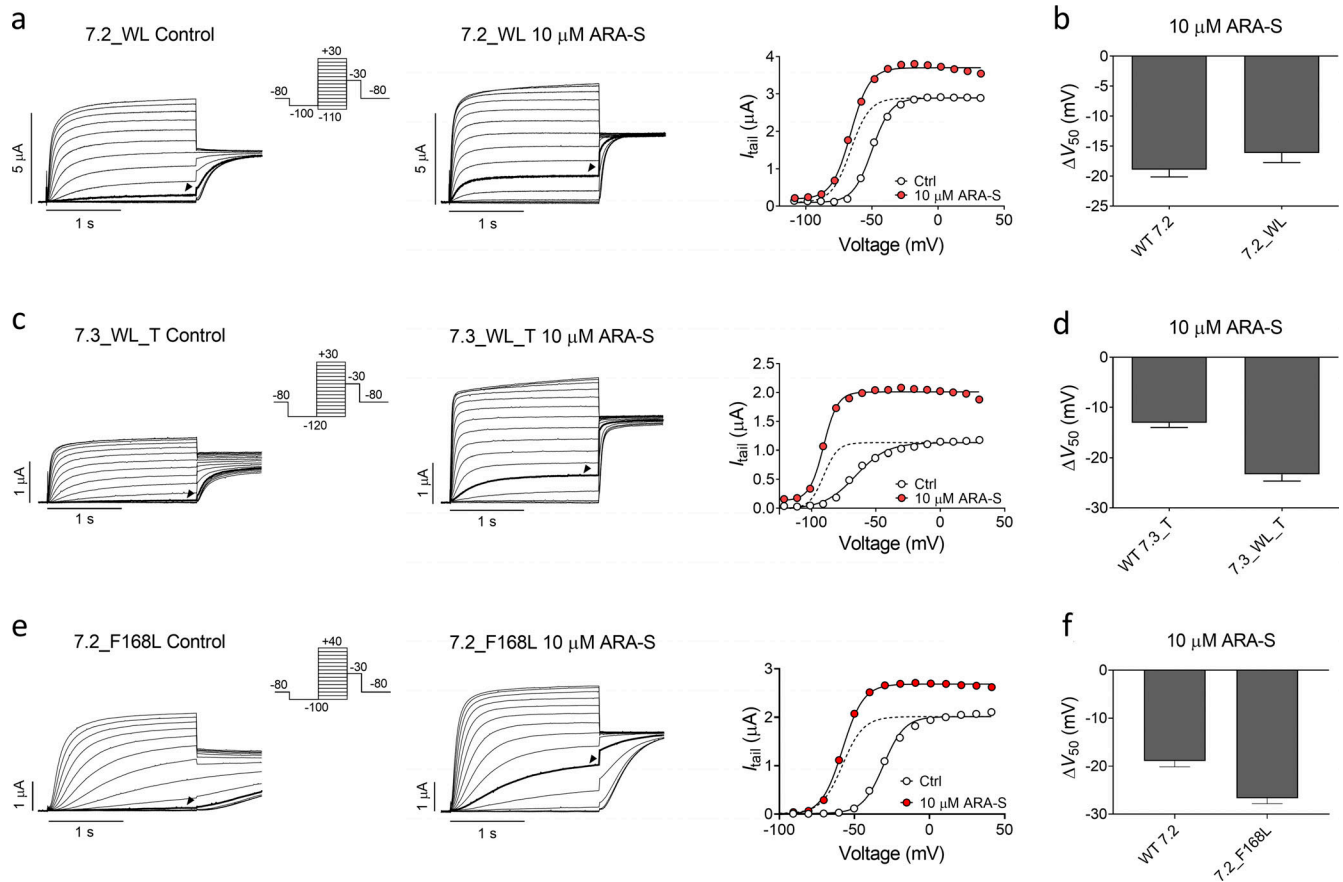
Figure S4. **ARA-S activates homomeric hK$_V$7.2 and hK$_V$7.3 tryptophan mutants. (a)** Representative current traces and corresponding $G(V)$ curve of hK$_V$7.2_W236L before and after application of 10 µM ARA-S. Arrowheads in the current families indicate an activating voltage step to −60 mV. Insert of used voltage clamp protocol. Dashed line in the $G(V)$ curve shows the curve for 10 µM ARA-S normalized to G_{MAX} of control. **(b)** Mean shift in V_{50} induced by 10 µM ARA-S on WT hK$_V$7.2 and hK$_V$7.2_W236L. Data shown as mean ± SEM; n = 6–10. **(c and d)** Same as in a and b, but for WT hK$_V$7.3_A315T and hK$_V$7.3_W265L_A315T. n = 4–9. Arrowheads in the current families indicate an activating voltage step to −80 mV. **(e and f)** Same as in a and b, but for WT hK$_V$7.2 and hK$_V$7.2_F168L. n = 6–10. Arrowheads in the current families indicate an activating voltage step to −50 mV. WL, tryptophan to leucine mutation.

Larsson et al.
Combined targeting of the M-channel

Journal of General Physiology   S4
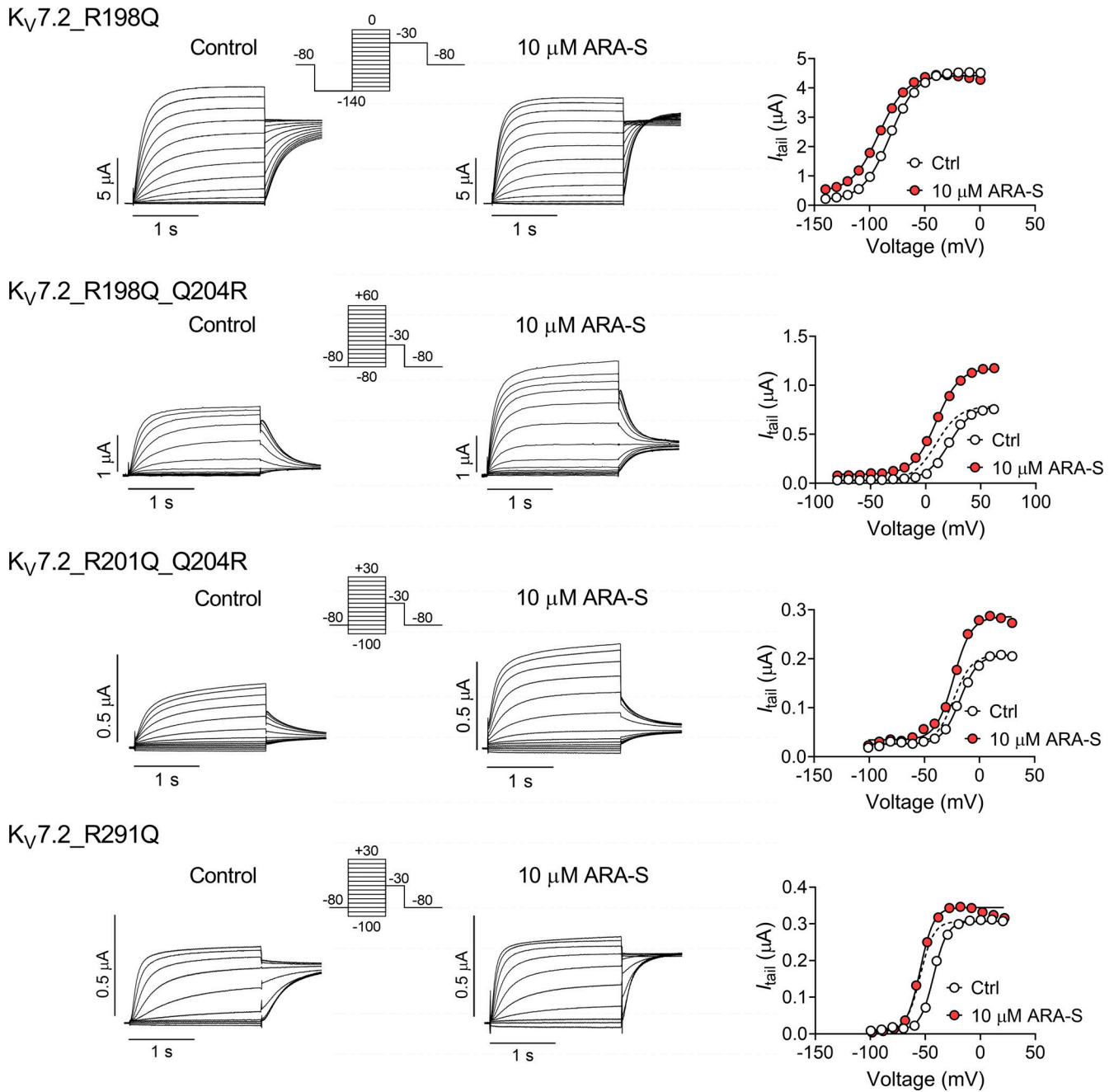https://doi.org/10.1085/jgp.202012576

Figure S5. **Specific charge-neutralizing mutation in hK$_V$7.2 reduces ARA-S effect.** Representative current traces and corresponding $G(V)$ curve for indicated mutants before and after application of 10 μM ARA-S. Insert of used voltage clamp protocol. Note the unstable current amplitude of hK$_V$7.2_R198Q, which prevented G_{MAX} determination.
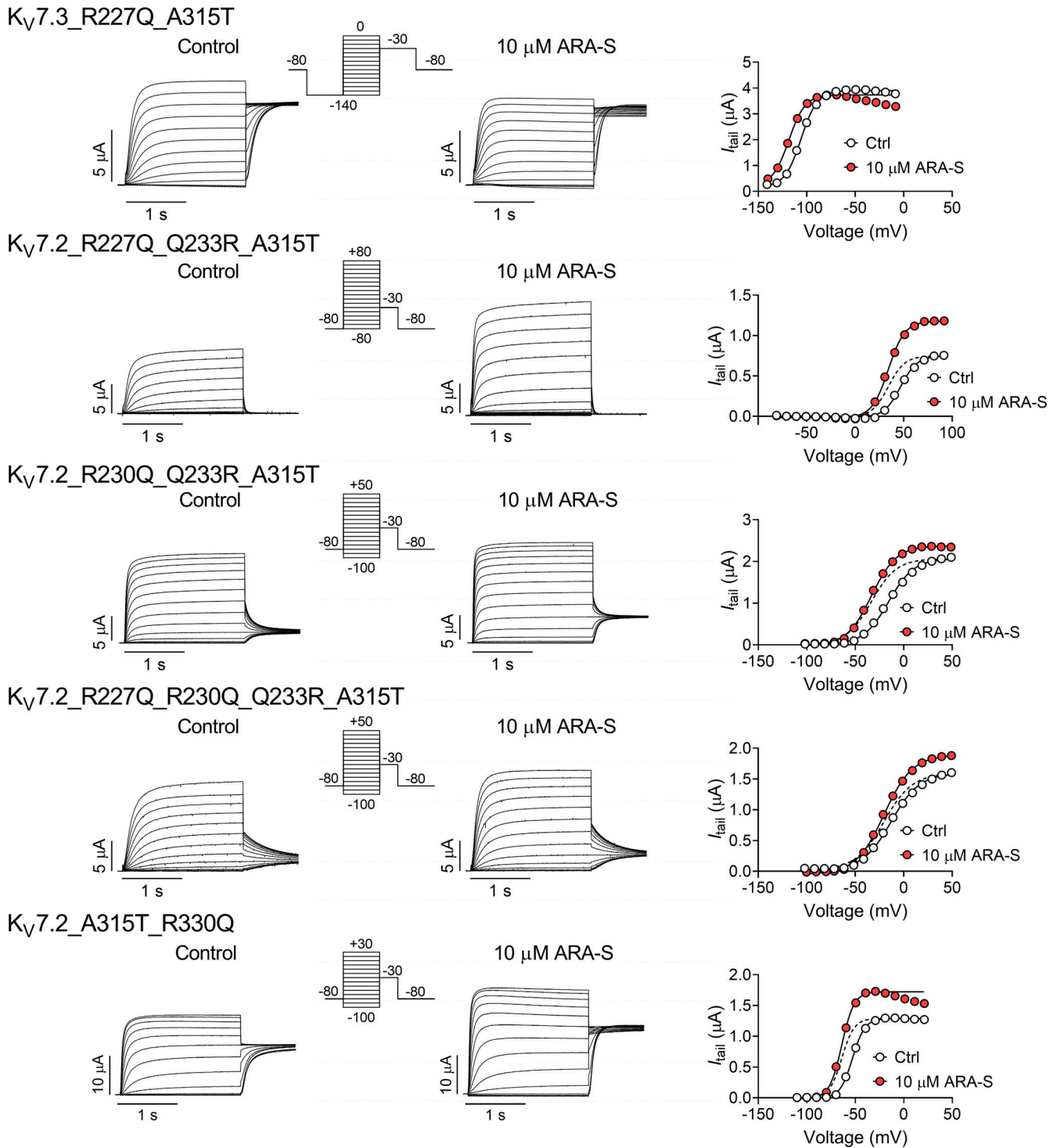
Figure S6. **Specific charge-neutralizing mutation in hK$_V$7.3 reduces ARA-S effect.** Representative current traces and corresponding G(V) curve for indicated mutants before and after application of 10 μM ARA-S. Insert of used voltage clamp protocol. Note the unstable current amplitude of hK$_V$7.3_R227Q_A315T, which prevented G$_{MAX}$ determination.
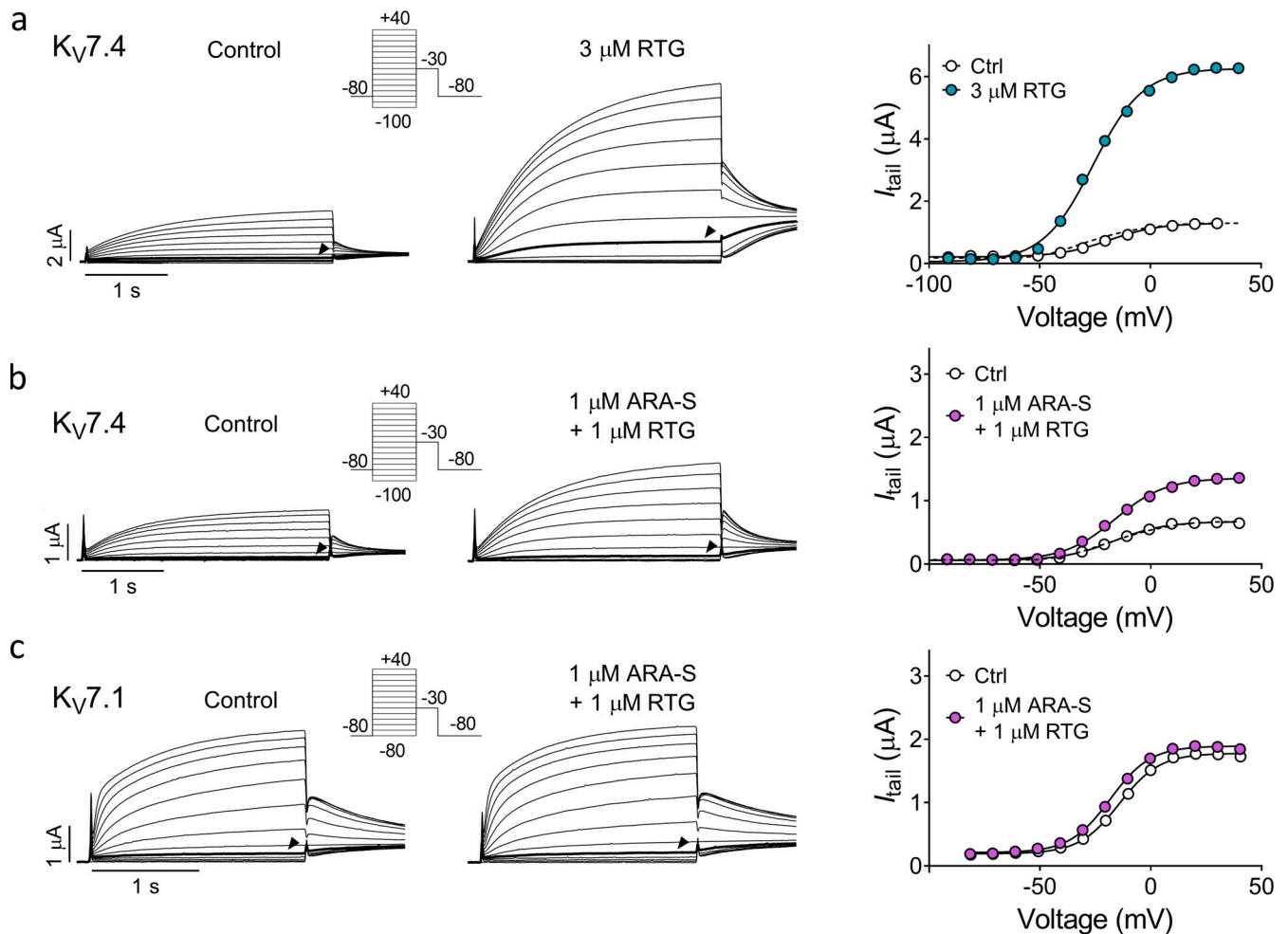
Figure S7. **Coapplication of low concentrations of ARA-S and retigabine limits the off-target effect on other hK$_V$7 subtypes. (a and b)** Representative current traces and corresponding $G(V)$ curves for hK$_V$7.4 before and after application of either 3 µM retigabine (RTG; a) or coapplication of 1 µM ARA-S and 1 µM retigabine (b). Arrowheads indicate an activating voltage step to −40 mV. Insert of used voltage clamp protocols. **(c)** Representative current traces and corresponding $G(V)$ curves for hK$_V$7.1 before and after coapplication of 1 µM ARA-S and 1 µM retigabine. Arrowheads indicate an activating voltage step to −40 mV. Insert of used voltage clamp protocols. Dashed lines in the $G(V)$ curves show the curve for each test compound normalized to G_{MAX} of control.
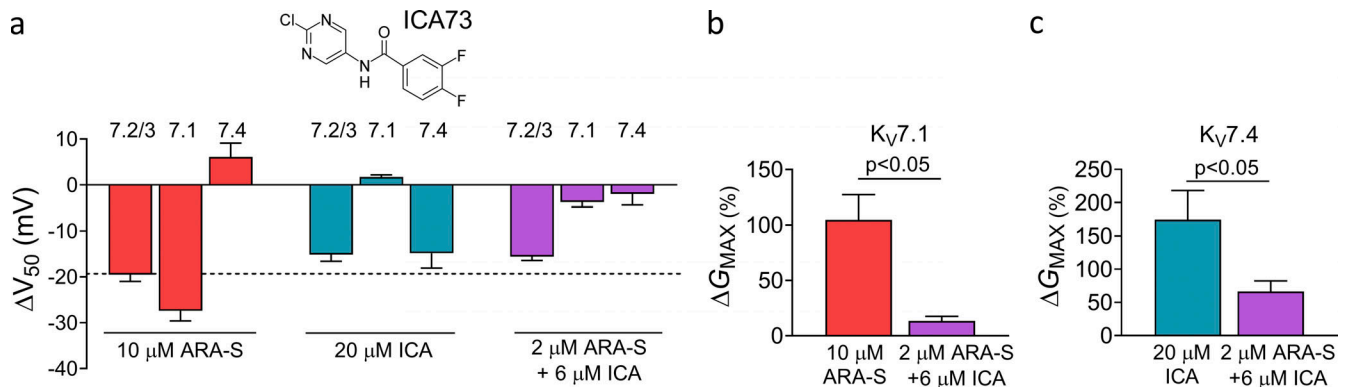

Figure S8. **Coapplication of low concentrations of ARA-S and ICA73 limits the off-target effect on other hK$_V$7 subtypes. (a)** Mean shift in V_{50} induced by 10 µM ARA-S, 20 µM ICA73 (structure shown), or 2 µM ARA-S + 6 µM ICA73 coapplied on indicated channels. Data shown as mean ± SEM; n = 4 or 5. Dashed line denotes a shift in V_{50} of −20 mV. **(b and c)** Mean increase in G_{MAX} of hK$_V$7.1 or hK$_V$7.4 induced by indicated treatment. Data shown as mean ± SEM; n = 4 or 5. Statistics denote Student's t test.

Table S1 summarizes the biophysical properties of used constructs.